Composite Structures 249 (2020) 112548

Contents lists available at ScienceDirect

Composite Structures

journal homepage: www.elsevier.com/locate/compstruct

Out-of-plane crushing response of aluminum honeycombs *in-situ* filled with graphene-reinforced polyurethane foam

Daniel Pietras [a,*], Emanoil Linul [b,*], Tomasz Sadowski [a,*], Alexis Rusinek [c]

[a] Department of Solid Mechanics, Lublin University of Technology, Nadbystrzycka 40 Str., 20-618 Lublin, Poland
[b] Department of Mechanics and Strength of Materials, Politehnica University of Timisoara, 1 Mihai Viteazu Avenue, 300 222 Timisoara, Romania
[c] Laboratory of Microstructure Studies and Mechanics of Materials, UMR-CNRS 7239, Lorraine University, 7 rue Félix Savart, BP 15082, CEDEX 03, 57073 Metz, France

ARTICLE INFO

Keywords:
Compression properties
Reduced graphene oxide flakes
Graphene-reinforced PU foams
In-situ foam-filled honeycombs
Energy absorption performances

ABSTRACT

This work reports the out-of-plane crushing response of aluminum honeycomb (HC) filled with polyurethane (PU) foams. For the filling of the HC, two types of PU foams were manufactured: unreinforced PU (UR/PU) foam and PU foam reinforced (GR/PU) with reduced graphene oxide (rGO) flakes. In this investigation, the static and low velocity impact compressive tests were performed on the separate constituents (UR/PU foam, GR/PU foam and empty HC) and their combinations (UR/PU foam-filled HC and GR/PU foam-filled HC). By the addition of 0.02% rGO flakes, to UR/PU, an increase (over 41%) of the strength and energy absorption properties was obtained. Moreover, due to the interaction effect, the foam-filled HC composite highlights better properties (up to 61%) than the empty HC structure. Further, it has been observed that exposure of the specimens to ultraviolet (UV) radiation do not change the foam density, but their properties increase by up to 30%. Finally, it was noticed that the *in-situ* foam-filled HC manufacturing technique is clearly superior to the *ex-situ* method, while the foam material dictates the filled HC collapse mechanisms considerably.

1. Introduction

The honeycomb (HC) structures and rigid polyurethane (PUR) foams are widely used in aerospace and marine industry as a core of sandwich composite structures [1–5]. The metallic HC structures found applicability in automotive industry as cushioning material. In the first mentioned application, their excellent strength-to-mass ratio is crucial whereas in second the high-energy absorption performances are essential. Especially in automotive industry, these lightweight structures are exposed to quasi-static and impact loading conditions. It is demand to found the new solutions, which will be able to improve the mechanical properties of currently used materials. The literature survey shows that combination of these materials is promising to fulfill the demand of the industry. The extensive investigations of nano- and micro-fillers in polymeric materials show that using them can also improve the mechanical properties of foams [6–8].

In the case of single thin-walled metallic tubes filled by foam materials was found that foam is changing the collapse mode from diamond shape for empty tubes (ETs) to concertina mode (progressive axisymmetric) in foam-filled tubes (FFTs) [9–11]. As a result of the "interaction effect" between foam and tube walls, the crushing load and energy absorption capacity of the composite structure are higher than the sum of accordingly properties of their constituents. This effect can be described by the following equation [12]:

$$P_{af} = P_{ae} + C \cdot \sigma_{pl} b^2 \quad (1)$$

where, P_{af} is the average crushing load of the FFT, P_{ae} is the crushing load of the ET, σ_{pl} is the plateau stress of the foam, b is the length of the tube and C is a strengthening coefficient. For one tube this coefficient is equal to C = 1.7, regardless of the type of used foam (aluminum or polystyrene) [13]. Similarly, the HC can be considered as a structure made of multiple thin-walled metallic tubes, due to this fact the composite HC-foam is promising to find application in the industry. Following this idea, a theoretical model for the crushing strength determination of foam-filled HCs was proposed in [14]. They observed that the crushing stress of the foam filled HCs it is about 30% higher than the sum of the crushing stresses of its corresponding components.

Numerical analyzes can be used to predict the mechanical properties of the proposed composites. To simplify complex geometric problems, plates and shell theories can be applied. A comprehensive review of these methods is presented in [15]. Most of the predictions are made using the finite element method, but no mesh techniques are still being

* Corresponding authors.
E-mail addresses: d.pietras@pollub.pl (D. Pietras), emanoil.linul@upt.ro (E. Linul), t.sadowski@pollub.pl (T. Sadowski).

https://doi.org/10.1016/j.compstruct.2020.112548
Received 17 March 2020; Revised 2 May 2020; Accepted 26 May 2020
Available online 30 May 2020

developed for modeling composite structures [16–18]. In addition, the predictions of composites response can be improved by considering the cracking problem as discussed in [19,20]. The advanced theoretical background to consider the most critical elements of composite like the interfaces of foam-metallic skin and metal-metal joints are discussed in [21]. The proposition of the numerical description of the honeycomb by using Lagrangian approach is presented in [22]. The authors achieved good agreements between the test in blast loading conditions and the numerical results. The interesting approach to predict the response to applied loadings of another orthotropic material based on the honeycomb structure is presented in [23].

It is necessary to know the response of considered composite structures to applied dynamic loadings. In the aerospace industry, the resistance to low rate impact is important in the case of tool drop during aircraft maintenance. On the other hand, in automotive and railway industries, more important is the response of these materials during high strain rate of loading is more important. In [22] the numerical model to investigate the sensitivity of the plateau stress to impact loading, in various configuration of honeycombs, was proposed. The authors used rate independent material. They assessed that the plateau stress is related to impact rate by conical curve. It is well known that solid material of honeycomb structure is rate dependent. The studies which taken into account this phenomenon are conducted in [23]. In model proposed by Tao et al [23], the plateau stress consist of 3 terms: static, strain rate and inertia term. The authors observed that the inertia term starts to be significant in very high strain rates. They conducted numerical analyses for 3 cases of HCs: for rate independent (RI) material, for the material with weak rate dependence (WRD) and for material with strong rate dependence (SRD). The results of these analyses indicate that at strain equal to 0.8 in case of WRD the stress is 55% higher in comparison to RI material, while for material with SRD the stress is 141% higher in comparison to RI material. Therefore, the material rate sensitivity is an important term in the HC structures response to applied loadings with high strain rates. The experimental study conducted in [24] indicates that sensitivity of HC structures to strain rate in range $10^{-3} \div 2{\cdot}10^{2}$ depends on cell-walls thickness to edge length t/l ratio. The rate sensitivity of honeycomb increases for higher t/l values. The constituent material of considered HC, the aluminum alloy 3000 series was investigated in [25]. The tests conducted in strain rates 0.1 s^{-1} to 9500 s^{-1} by using Split Hopkinson Pressure Bar indicate that at room temperature the yield stress at 20% strain increase by 60%. The curve that describes stress in function of strain rate is nonlinear and nonlinearity is more notable with strain rates higher than 10^{3} s^{-1}. The strain rate sensitivity is dependent on the temperature, namely it is higher at lower temperatures and it vanishes at 600 K (326 °C). The proposition of the numerical description of the honeycomb by using Lagrangian approach is presented in [26]. The authors achieved good agreements between the test in blast loading conditions and the numerical results. The interesting approach to predict the response to applied loadings of another orthotropic material based on the honeycomb structure is presented in [27].

The addition of graphene derivatives such as graphene nanopalettes (GNPs) and reduced graphene oxide (rGO) to thermoplastic rigid polyurethane (TPU) leads to the increase of the storage modulus. Pure TPU is characterized by constant storage modulus independent on strain magnitude. In case of usage the nanofillers the Payne effect occur, namely the storage modulus decreases together with the increase of strain [28]. This effect is caused mainly by filler-filler interactions and is stronger when the amount of filler increases. Santiago-Calvo and co-workers [29] studied the PUR foams produced from a polyol functionalized with GO. They found that the inclusion of the rGO particles reduces the thermal conductivity and mechanical performances of the PUR foam. It was also noticed that the inclusion of small amounts of graphene modifies the internal structure of the foam, reducing the size of cells by up to 33%. Yan et al [30] reported a study of PUR foam nanocomposites based on graphene nanosheets (GNSs). Contrary to [25], the authors found that, due to the wrinkled surface structure, higher specific surface area and unique 2D morphology, only 0.3 wt% GNSs content is optimal to improve the compressive modulus (by 36%) and heat resistance. They observed that the use of GNSs as reinforcements does not improve the thermal conductivity. Graphene with amine group can make the foam superhydrophobic, due this fact it can find the application in oil filter manufacturing [31]. It is possible to create more functional material [32], which will be able to conduct electrical current and will be pressure sensitive. The graphene is strongly immobilized in polyurethane structure by chemical links. The successful using the GNPs is reported in [33]. The addition 1% and 2% of graphene nanofiler to elastic foam causes the increase of the apparent density, higher tensile strength, higher hardness, and higher storage modulus at low temperature but it has no influence on thermal stability of the material.

Most of the mentioned works studied the mechanical behavior of the PUR foams or the HC structures separately, less both of them, e.g. [34]. As it was noticed, the mechanical, physical and thermal behavior of the graphene-reinforced foams or of the empty HCs is well known, even of the HCs filled with the regular/unreinforced foams. As shown in [12,35,36], the adhesion between the walls of metallic sections and foam materials leads to a significant increase of the strengthening effect. To the best knowledge of the authors, no literature evidence was found regarding the compression behavior of HC filled with graphene-reinforced PUR foam. Therefore, this paper aims to investigate the out-of-plane mechanical properties and energy absorption performances of new composites under quasi-static and impact loading conditions. For this purpose, two methods of filling the HC structure with PUR foam improved by rGO are investigated, the best one being exploited in this work. Furthermore, comparisons with the regular foam-filled HC structures are presented together with the collapse mechanisms. Finally, the compressive behavior of the investigated structures during UV irradiation is investigated. The new foam-filled HC composite aims to increase the efficiency in energy absorption of the materials in automotive, railway and aircraft applications.

2. Materials and methods

2.1. Materials

The proposed composites were made of commercially available semi-finished products used in industry to increase the chances of finding applications quickly.

2.1.1. Polyurethane foam

The foams were prepared by employing two-component commercial system that is the rigid polyurethane *(PU)* foam PUR 2 K 90. Fig. 1 show a SEM image of the microstructure of prepared foam.

2.1.2. Aluminum honeycomb

The double walled hexagonal honeycomb *(HC)* can be classified as a lightweight thin-walled structure. The commercial expanded HC panels (CEL Components S.r.l.) with 3.2 mm cell size and a nominal density of 128 kg/m^3 were used. The average cell-walls thickness is t = 0.07 mm. The considered HCs are manufactured of 3000 series aluminum alloy. This aluminum and manganese alloy is commonly used in industry.

The macroscopic observation of considered HC panel is shown in Fig. 2. The structure of HC has a huge impact on their mechanical properties. The influence of cells dimensions and the thickness of ribbons is obvious, but the cells fillet radius and some geometrical imperfections are often omitted, especially in numerical modeling [37]. These parameters also have a huge impact on response of the HC to

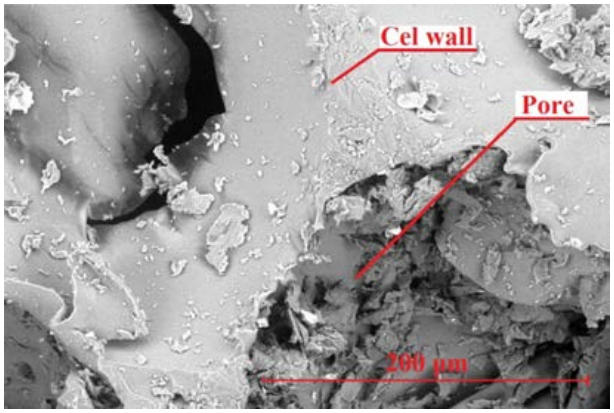

Fig. 1. The microstructure of considered foams.

applied compressive loadings. In considered HC, the average cells dimensions are $d_1 = 5.819$ mm with standard deviation $n = 0.134$ mm, and $d_2 = 4.516$ mm with $n = 0.065$ mm.

The average length of the bonding of ribbons is $d = 1.075$ mm, with a standard deviation of $n = 0.068$ mm. The fillet radius has similar average value to the ribbon thickness $r = 0.816$ mm, but possesses largest deviation. The ribbons in the height direction have visible imperfections in form of dents. They have diameter close to 0.3 mm and are located uniformly in each cell in approximate distance of 6 mm.

2.1.3. Reduced graphene oxide

The reduced graphene oxide (rGO) flakes, manufactured by Institute of Electronic Materials Technology (Warsaw, Poland) were used. The rGO flakes are hydrophobic and stable in air environment. The assessed by manufacturer bulk density is 0.019 g/cm^3 whereas the specific surface area equals 266 m^2/g. Mainly, it consist of carbon (70–80%) and oxygen (15–20%), rest is completed by sulfur and hydrogen (<2%) and nitrogen (<0.3%). The rGO flakes can be obtained by chemical reduction of graphene oxide using benzylamine as reducing and stabilizing agent [38]. The rGO can also be obtained by treatment the graphene oxide by UV irradiation, compatible with sunlight spectrum [39].

2.2. Specimens preparation

2.2.1. Unreinforced polyurethane foams

The constituents called by manufacturer as “foam” and “curing agent” (polyol and isocyanate) were mixed in proportions 100:115 (weight), (1:1 by volume). For obtaining the *Unreinforced Polyurethane (UR/PU) foam* specimens, in one preparation was used 100 g of foam and 115 g of curing agent were used. Before measuring the appropriate amount of constituents, the contents of the main containers were thoroughly mixed because the ingredients might sediment. All of operations were performed at room temperature and normal humidity conditions. The constituents were mixed using a spoon; afterwards the substance was poured to the 140 mm × 170 mm × 140 mm box where the expansion started. During expansion process the box was placed in water with temperature 18(±2)°C to avoid sudden increase of temperature during foam curing. Subsequently after 24 h, the foam was cut into specimens.

The repeatability of the UR/PU foam specimens height, which is crucial during the experimental tests, was achieved by placing the pre-trimmed foam specimens between the aluminum guides and trimming with sandpaper stuck on a flat surface. The specimen dimensions were adjusted to obtain compressive forces possible to measure with proper ratio between noise to signal and to satisfy the representative volume element, more than 9 cells in each direction [40,41].

2.2.2. Reinforced polyurethane foams

To manufacture the *Graphene-Reinforced Polyurethane (GR/PU) foam* specimens, the rGO flakes were added as 0.02% sum of mass the liquid foam constituents. The real content can be a little bit smaller due to some loses and concentration near the mold walls caused by the process of foam expansion. The constituents of PU foam have different viscosities. To facilitate the mixing process, the rGO flakes were added to isocyanate constituent, which has smaller viscosity. Mixing graphene particles with isocyanate component was performed by 24 kHz, 400 W ultrasonic mixer. The ultrasonic mixer elevated the temperature of fluid during the operation. When the isocyanate constituent is mixed with the polyol constituent the chemical reaction starts. In case of PU foam fabrication the initial temperature of constituents is important since the polymerization reactions are exothermic, meaning it produces heat. As the chemical reaction progresses, the viscosity of the mixture will also increase. This increase continues during the foaming process until the reacting liquid turns into the PU solid at the end of the reaction. Too high initial temperature can lead to the destruction of the internal structure during foam expansion process. The trials with immediately mixing the graphenized isocyanate with polyol were unsuccessful, due to this fact after the mixing of graphene particles constituent was cooled to room temperature (20 °C) and after that the foam was manufactured. The cellular materials properties are strongly sensitive to the porosity of the material. Using the rGO flakes in the manufacturing process can increase the porosity of the foam, which may lead to wrong interpretation derived test results.

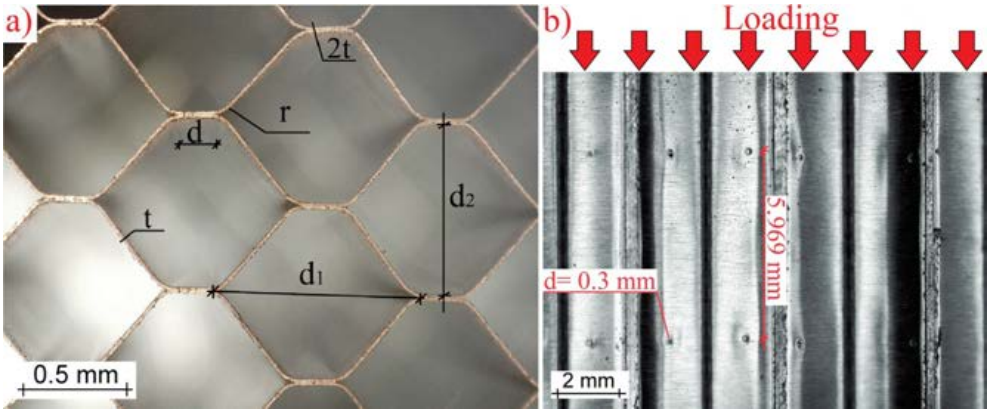

Fig. 2. The macrostructure of considered HC: top view (a) and side view (b).

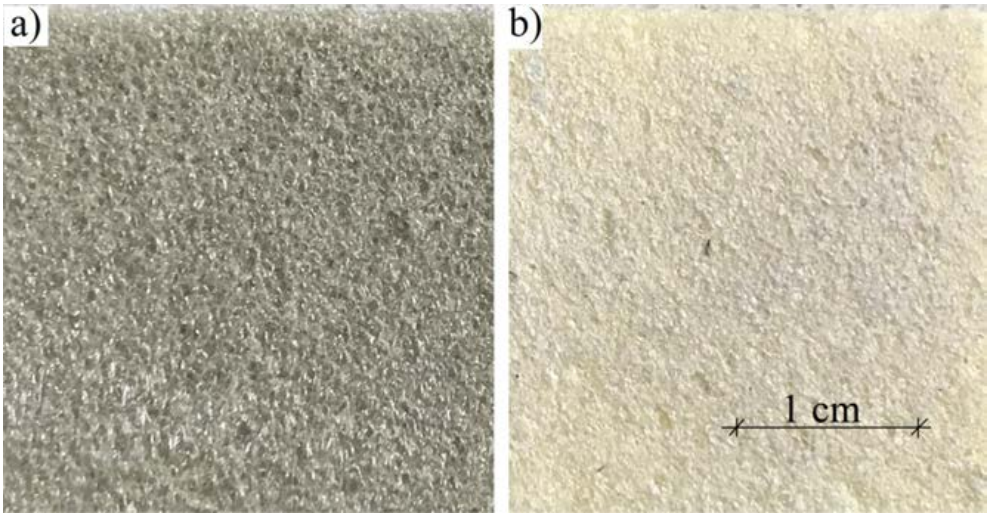

Fig. 3. Macroscopic comparison of the GR/PU (a) and UR/PU (b) foam specimens.

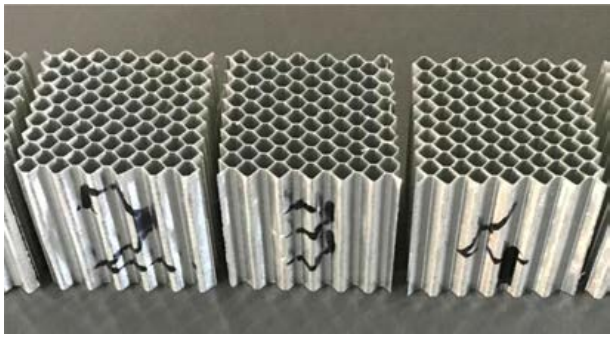

Fig. 4. The E-HC specimens together with cells pattern.

The manufacturing conditions were adjusted and the specimens were selected to obtain the as close as possible UR/PU and GR/PU densities.

The obtained GR/PU foam specimens have macroscopically the same structure with UR/PU ones, and the only difference is the color, as shown in Fig. 3.

2.2.3. Empty aluminum honeycomb

In this study, the *Empty Aluminum Honeycomb (E-HC)* specimens were cut to obtain the same number of ribbons as well as cells in each specimen. The number of cells was chosen to obtain the shape of specimens as close as possible to cube (with a side length of approximately 40 mm). It was 8 full cells in direction perpendicular to ribbons and 11 full cells in ribbon direction. Fig. 4 presents the obtained E-HC specimens.

The industrial grade of HC panel has some imperfections in the shape of the cells, due to unequal expansion process, and some tolerances of manufacturing process. Therefore, the prepared specimens have a little bit various dimensions. It is possible that sometimes the parallelism of the edges is not maintained, because of this the length measurements was performed in the middle of each edge. The parallelism is preserved between the supporting surface of the specimen and the loading surface. The undesired ribbons were manually removed, while in direction perpendicular to ribbons the specimens were cut in precision cutting machine Struers Secotom 10.

2.2.4. Foam filled honeycombs

The HC specimens, used to fill by *UR/PU* and *GR/PU*, were prepared in the same way like *E-HC*. The HC specimens filled with

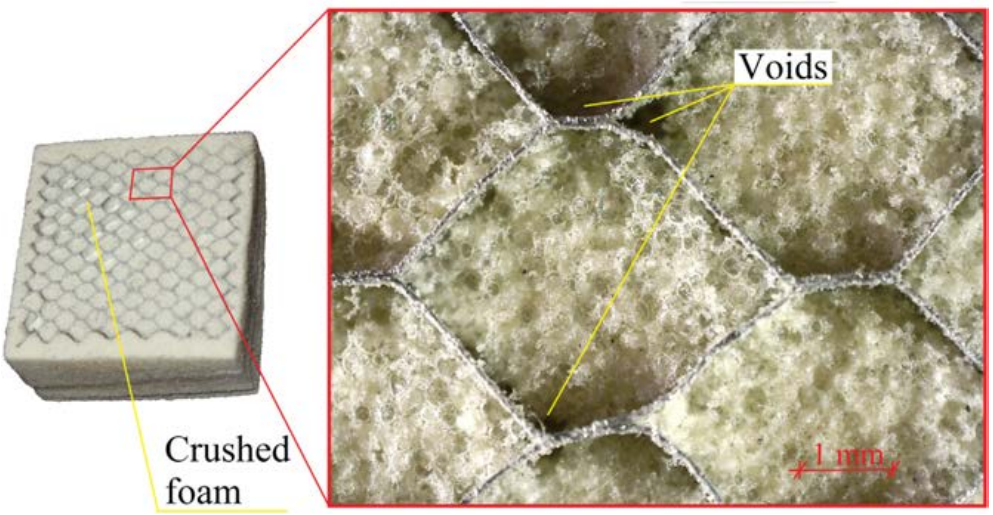

Fig. 5. The *ex-situ* filled HC specimen obtained by the pressing the PU foam.

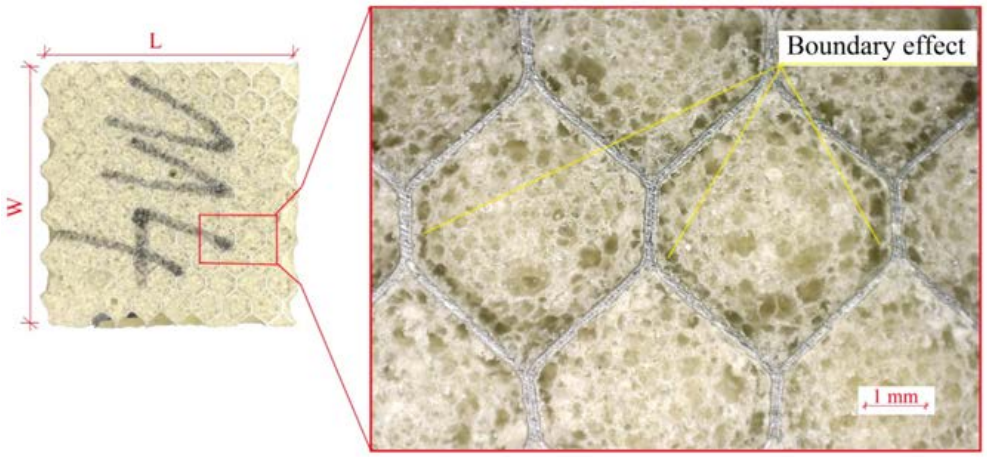

Fig. 6. The *in-situ* filled HC specimen obtained by immersing HC in the PU foam liquid mixture.

UR/PU foams are called *Unreinforced Polyurethane Foam Filled Honeycomb (UR/PU-HC)* composites, while those filled with GR/PU foams are named *Graphene-Reinforced Polyurethane Foam Filled Honeycomb (GR/PU-HC)* composites. It was checked two methods to fill the cells of HC by the polyurethane foam: an *ex-situ* and an *in-situ* method. The fist, *ex-situ* method, is by pressing of the expanded and hardened foam into the HC cells. This way turned out to be unreliable. Between the HC walls and PU foam, it was possible to observe voids, visible in Fig. 5. The foam was also compressed in some cells. In addition, the foam can be removed easily from the HC cells when this method is used.

In the second, *in-situ* considered method, the HC panel was placed on the flat surface of the mold. The liquid compound of foam was slipped from top part of the HC. This operation was carried out carefully to fill all cells of the HC panel. After the curing process, the foam was gently cut around the HC cube. The resultant specimen achieved by this method is shown in Fig. 6. It should be mentioned that curing process of foam which expanded in HC is longer than in case of free foam due to fact that the air flow and moisture penetration is obstructed.

In the cell walls vicinity, the expansion process is a little bit disturbed. This effect is observed also in huge molds and free edges of cured foam. At the interface between the foam and mold a continuous layer of polyurethane is usually formed. In case of HC panel, each cell is a separate mold with its own interfacial continuous film. Therefore, in Fig. 6 it can observed the changes in internal structure in this region. The boundary effect is small in comparison to cell dimension. In the considered specimens, the foam is properly bond to HC surfaces.

2.3. Methods

2.3.1. Basic measurements

The dimensions of the specimens are measured by caliper with a precision of 0.01 mm. The masses are measured by Ohaus PA214/1

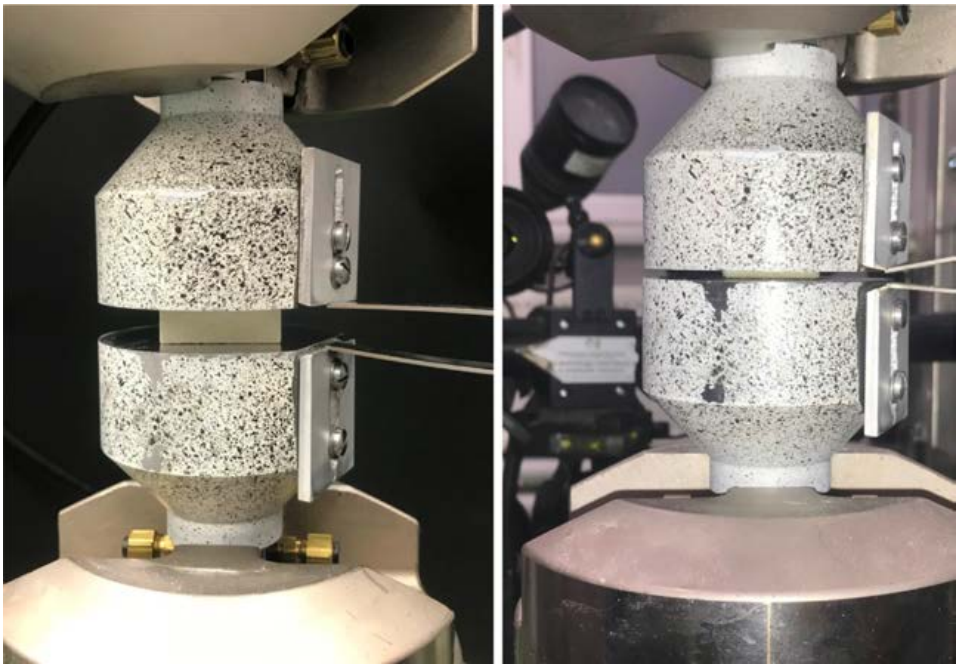

Fig. 7. Fixing the specimen under quasi-static condition: before (left) and after (right) compression test.

balance with a precision of 0.0001 g. The strains of specimens in quasi-static tests are measured by MTS Clip-On Gauge. The microstructure of HC was analyzed by Quanta Check 300 microscope.

2.3.2. Quasi-static tests

The quasi-static compression tests were carried out on 25 kN MTS Bionix hydraulic universal testing machine. The high-strength steel grips for compressive tests were mounted into the standard tensile grips. The surfaces of the grip were polished to reduce the friction effects. As shown in Fig. 7, for measuring the specimens deformation, the Clip-On gage gauge mounted to the rigid steel grip was used. It allows to measure more preciously the load displacement, without the machine stiffness influence to define more precisely the strain level applied as it is a soft material.

The compression tests were conducted under 3 mm/min constant rate of machine piston displacement, according to ISO 13314-11 standard [42].

2.3.3. Impact tests

The impact tests were performed by using Instron dynatup drop tower with 45 kN force transducer. The mass was set to 15.643 kg for the empty HC and to 27.8735 kg for the foam filled HC. The impacts were conducted with the initial velocity close to 5 m/s. This velocity give the strain rate equal to 125 s^{-1}.

2.3.4. Ultraviolet (UV) tests

The ultraviolet (UV) radiation tests were prepared by using Accelerated Weathering Tester delivered by the Q-Lab Corporation. UVA-340 lamps were used since they generate waves that are similar to sunlight ones. The spectrum covers the G177 standard [43]. The spectrum is shown in Fig. 8.

The specimens were sealed to the aluminum holders by double-sided tape. The power of radiation was set to 0.72 W/m^2. The temperature in the chamber was 50 °C. Total test duration was 96 h. In each 24 h, the specimens were rotated to obtain the uniform distribution of the volume exposed to UV radiation. It was observed that without rotation the surface sealed to the holder was protected against the UV radiation.

2.3.5. Data evaluation

The investigated polyurethane foams (UR/PU and GR/PU foams), empty honeycombs (E-HC structure) and foam-filled honeycombs (UR/PU-HC and GR/PU-HC composites) exhibit loading compressive behavior similar to cellular materials [44–46]. This mechanical response consists of a very small linear elastic region up to the critical loading force (where the compressive strength is obtained), followed by a very large plateau region which is responsible for high-energy absorption capabilities. The characteristic curve ends with the densification region, where the cell walls or pores get in touch with each other and the material responds to the applied loads as a bulk material [47,48]. The graphical representation of cellular materials response under compressive load is shown in Fig. 9.

The main differences between the behavior of different types of cellular materials is represented by the ratio between compressive strength (σ_{max}) and plateau stress (σ_{pl}), the length of the plateau region (l_{pl}) and their shape (i.e. absolutely flat or with some hardening).

Using the geometric parameters (length, width and height) of the manufactured samples, following compression tests, the stress (σ), energy absorption (W) curves depending on strain (ε) were obtained. The W of the samples was determined by Eq. (2), using variable integration limits [42,49,50]:

$$W = \int_0^{\varepsilon_d} \sigma d\varepsilon \tag{2}$$

where ε_d is the strain in which energy efficiency reaches maximum value. This strain is so-called densification strain. The compressive properties of investigated PU foam samples were determined according to ISO 13314-11 standard [38]. These properties are represented by *compressive modulus (E)*-determined from the linear-elastic region of the σ-ε curve, *yield stress* (σ_y) or *first maximum compressive strength* ($\sigma_{max} = \sigma_y$)-the first peak point at which the first increase in strain is obtained without the increase in stress, *plateau stress* (σ_{pl})-determined as the arithmetic mean of stresses corresponding to 20% and 40% strains, *densification strain* (ε_d), σ corresponding to ε_d (σ_d), W corresponding to ε_d (W_d) and energy absorption efficiency corresponding to ε_d (η_d).

The energy absorption efficiency (η) represents the ratio between W and the product of the upper limit of the compressive strain (ε_0) and the compressive stress at the ε_0 (σ_0) [42,51,52]:

$$\eta = \frac{\int_0^{\varepsilon} \sigma d\varepsilon}{\varepsilon_0 \times \sigma_0} \tag{3}$$

The ε_d, σ_d, W_d and η_d properties were determined based on energy absorption efficiency (η).

The sample density (ρ) was calculated by dividing the sample mass (m) by its volume (V). The samples with ρ below or above the 10% of the average of the densities per sample groups were excluded before experiments were conducted.

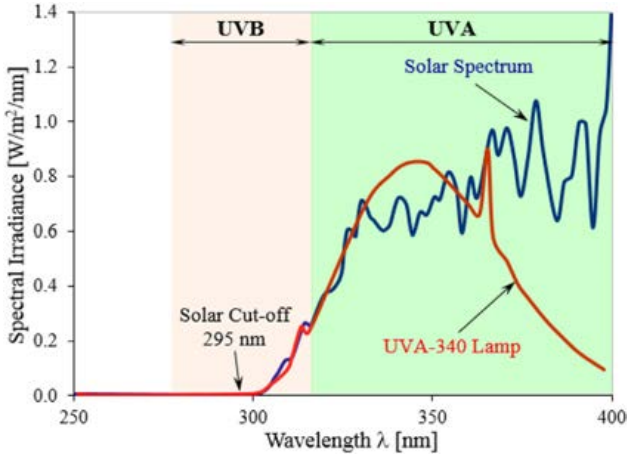

Fig. 8. The spectrum used in the UV radiation test.

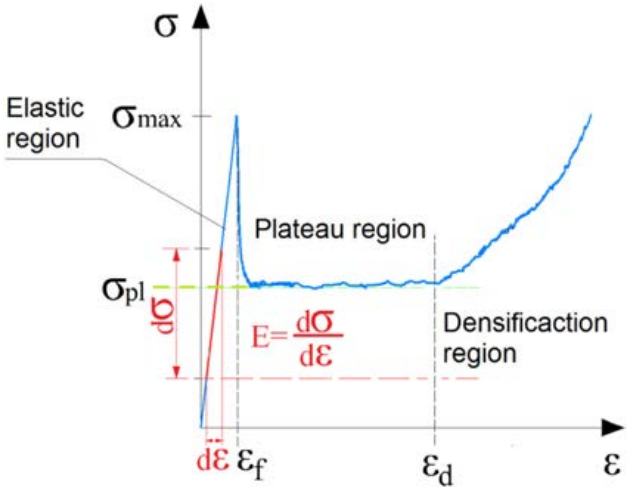

Fig. 9. The typical compression response of cellular materials.

3. Results and discussions

3.1. Physical properties

To determine the density of samples, before performing the experimental tests, all the samples were measured and weighed. Tables 1–3 shows the main physical properties of all UR/PU, UR/PU, E-HC, UR/PU-HC and GR/PU-HC samples manufactured for this investigation.

The mean apparent density (ρ) values are listed in Tables 1–3 according to sample type. Of the investigated foams, the smallest deviation was found for GR/PU foam, having a maximum value of 4.1%. On the contrary, UR/PU foam showed a standard deviation of 9.5%. As for HC composite structures, it seems that UR/PU foam flows more easily through HC cells, resulting in a maximum deviation of 3.4%. Even so, the GR/PU-HC samples exhibit insignificantly larger average deviations (of about 5.2%) than the UR/PU-HC ones. Due to very regular cellular structure of the HC, compared to the other types of

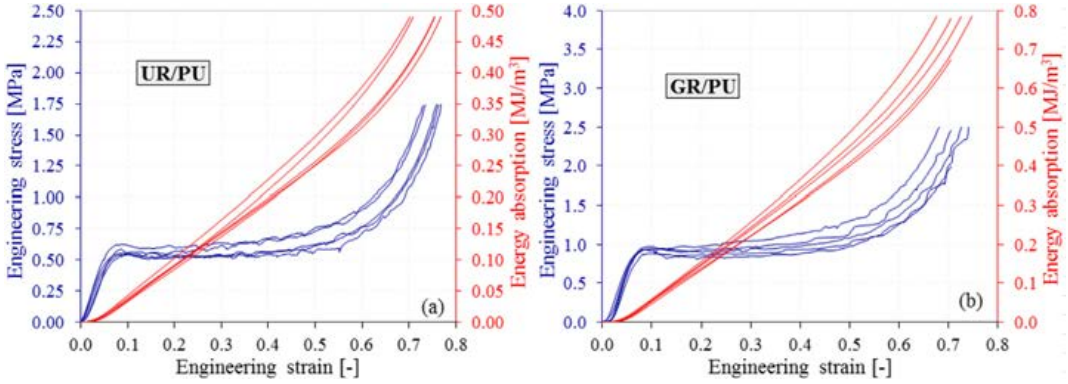

Fig. 10. Stress-strain and energy absorption-strain curves of UR/PU (a) and GR/PU (b) foams.

Table 1
Physical properties of investigated UR/PU and GR/PU foam samples.

Sample type	Sample number	Length [mm]	Width [mm]	Height [mm]	Volume [cm^3]	Mass [g]	Density [kg/m^3]
UR/PU	UR/PU1	27.28	27.28	11.18	8.320	0.8208	98.652
	UR/PU2	27.52	27.29	11.30	8.487	0.8512	100.300
	UR/PU3	27.54	25.27	11.65	8.108	0.9599	118.394
	UR/PU4	27.50	27.42	11.34	8.551	0.9156	107.076
	UR/PU5	26.95	27.37	11.42	8.424	0.9771	115.995
GR/PU	GR/PU1	39.68	39.92	11.20	17.741	1.893	106.718
	GR/PU2	35.14	33.83	11.17	13.279	1.359	102.314
	GR/PU3	31.65	32.18	11.15	11.356	1.189	104.665
	GR/PU4	32.36	34.10	11.03	12.171	1.235	101.443
	GR/PU5	32.92	34.63	11.04	12.586	1.374	109.139

Table 2
Physical properties of investigated E-HC samples.

Sample type	Sample number	Length [mm]	Width [mm]	Height [mm]	Volume [cm^3]	Mass [g]	Density [kg/m^3]
E-HC	E-HC1	39.40	40.94	40.00	64.521	6.165	95.553
	E-HC2	39.97	39.43	39.97	62.993	6.103	96.878
	E-HC3	40.57	39.98	40.06	64.977	6.182	95.138
	E-HC4	39.57	40.19	39.98	63.581	6.164	96.944
	E-HC5	40.17	40.30	40.08	64.884	6.144	94.699

Table 3
Physical properties of investigated UR/PU-HC and GR/PU-HC foam samples.

Sample type	Sample number	Length [mm]	Width [mm]	Height [mm]	Volume [cm^3]	Mass [g]	Density [kg/m^3]
UR/PU-HC	UR/PU-HC1	39.73	40.13	39.91	63.631	13.172	206.998
	UR/PU-HC2	40.68	41.03	39.97	66.714	13.219	198.149
	UR/PU-HC3	40.54	39.91	39.90	64.556	13.494	209.033
	UR/PU-HC4	40.53	40.33	39.92	65.252	13.404	205.418
	UR/PU-HC5	40.22	40.07	39.95	64.384	13.282	206.289
GR/PU-HC	GR/PU-HC1	40.26	40.30	39.96	64.834	13.267	204.623
	GR/PU-HC2	40.18	41.01	40.19	66.224	13.356	201.675
	GR/PU-HC3	39.87	40.64	39.94	64.715	14.338	221.553
	GR/PU-HC4	40.01	40.76	39.93	65.118	14.343	220.254
	GR/PU-HC5	40.48	40.13	39.88	64.784	14.002	216.135

samples (UR/PU, UR/PU, UR/PU-HC and GR/PU-HC), the E-HC samples showed the smallest deviation of about 1.2%. The average apparent density of the UR/PU-HC is 114% higher than E-HC and 93.8% higher than average density of UR/PU. The sum of the average apparent densities of both composite constituents: E-HC and UR/PU, is 1.73% smaller than effective density of composite: UR/PU-HC. This fact may be caused by presence of foam-aluminum interfacial layers.

3.2. Mechanical properties

3.2.1. Polyurethane foams

Fig. 10 presents the stress-strain and energy absorption-strain curves of investigated UR/PU and GR/PU foams. The relations shown in Fig. 10a indicate that prepared UR/PU foam samples have high repeatability. At the beginning of loading process, the response of the material is quasilinear. Near to first peak stress (around 0.5 MPa) the damage of internal structure of the samples starts and relation $\sigma(\varepsilon)$ is curved. Subsequently the plateau region occurs, being almost flat up to 30% strain. Between 30% strain and the onset strain of densification, the plateau region presents a slight hardening [53,54].

In the case of GR/PU foams, the beginning of the stress-strain relation is the same. The crucial difference is that the critical level of loadings is higher than in the case of UR/PU foam. The post failure behavior is also different in comparison to GR/PU foam. The region after critical failure is not flat but it is clearly visible that hardening

Table 4
Main quasi-static properties of UR/PU and GR/PU foams.

Foam type	Sample number	E [MPa]	σ_y [MPa]	σ_{pl} [MPa]	σ_d [MPa]	ε_d [%]	W_d [MJ/m^3]	η_d [–]
UR/PU	UR/PU1	10.055	0.586	0.541	0.563	55.11	0.281	0.499
	UR/PU2	10.179	0.542	0.619	0.876	58.80	0.323	0.403
	UR/PU3	11.124	0.556	0.547	0.642	53.71	0.281	0.437
	UR/PU4	9.691	0.545	0.543	0.707	58.09	0.306	0.433
	UR/PU5	12.032	0.533	0.539	0.622	52.94	0.268	0.430
GR/PU	GR/PU1	20.741	0.944	0.978	1.269	56.00	0.525	0.414
	GR/PU2	19.389	0.952	0.899	1.120	56.29	0.476	0.425
	GR/PU3	22.342	0.971	0.940	1.162	54.24	0.483	0.416
	GR/PU4	21.567	0.933	0.855	1.118	56.83	0.472	0.422
	GR/PU5	19.067	0.941	1.054	1.136	53.29	0.530	0.392

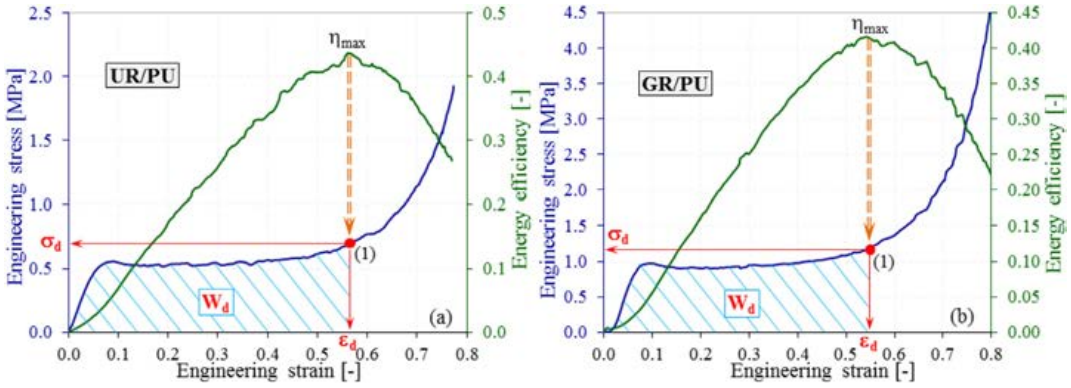

Fig. 11. Stress-strain and energy efficiency-strain curves of UR/PU (a) and GR/PU (b) foams.

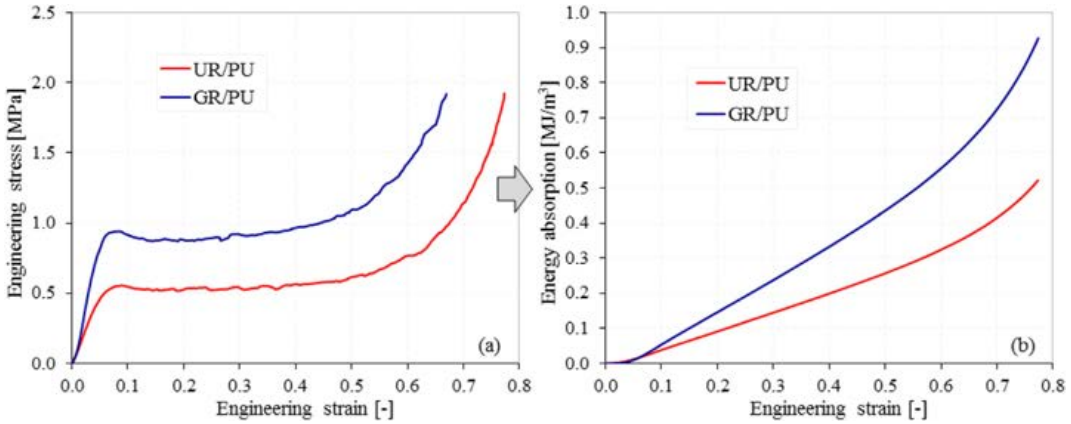

Fig. 12. Stress-strain (a) and energy absorption-strain (b) curves of UR/PU and GR/PU foams.

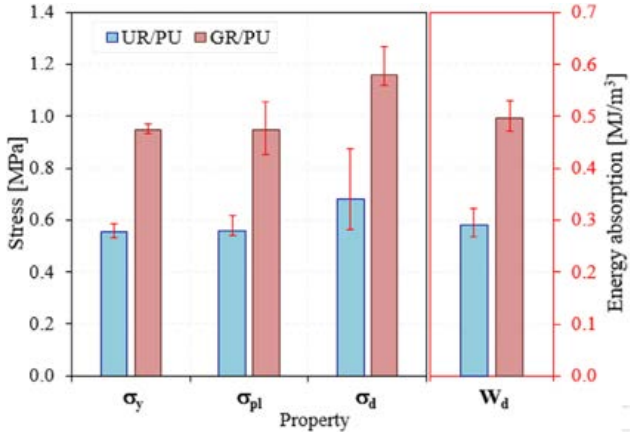

Fig. 13. Strength and energy absorption properties of UR/PU and GR/PU foams.

process starts immediately after the yield point (about 10% strain). Therefore, the GR/PU foams are able to absorb more energy than the corresponding UR/PU foams. In order to see more easily the differences between the main mechanical properties of the UR/PU and GR/PU foams are summarized in Table 4, according to the foam type.

In the Fig. 11, the most representative curves from each characteristic group of specimens are selected. Initially the maximum value of η from the energy efficiency-strain curve is determined (η_{max}), after which the strain corresponding to η_{max} is found (being actually ε_d). The other three properties (σ_d, W_d and η_d) are obtained by simply identifying the values corresponding to a previously found strain (ε_d).

For an easier comparison of the compression behavior of the UR/PU and GR/PU foams, Fig. 12 presents the stress-strain and energy absorption-strain curves of the investigated properties. From Fig. 12 it can be easily seen that both the strength and energy absorption properties differ significantly between the two types of foams.

The strength and energy absorption properties of UR/PU and GR/PU foams are shown in Fig. 13. It was found that compressive strength, plateau and densification stresses, and energy absorption performances are over 41% higher for GR/PU foams than for UR/PU foams. Moreover, in the case of the compressive modulus this difference increases even more, reaching 48.5% in favor of the GR/PU foams. Densification strain represents the only characteristic of compression that is approximately equal for both foams, being 0.7% higher in the case of UR/PU foams (see Table 4). Therefore, the presence of graphene in the PU foam structure leads to a considerable increase of the main properties.

From the literature, regardless of the matrix material (polymeric, metallic or ceramic), it is well known that the density is an important parameter that influences the behavior of the cellular materials [55–58]. Thus, it is very important to study how much this parameter influences each type of foam individually. Considering this aspect, Fig. 14 presents the variation of elastic (compressive modulus), strength (yield, plateau and densification strain) properties and energy

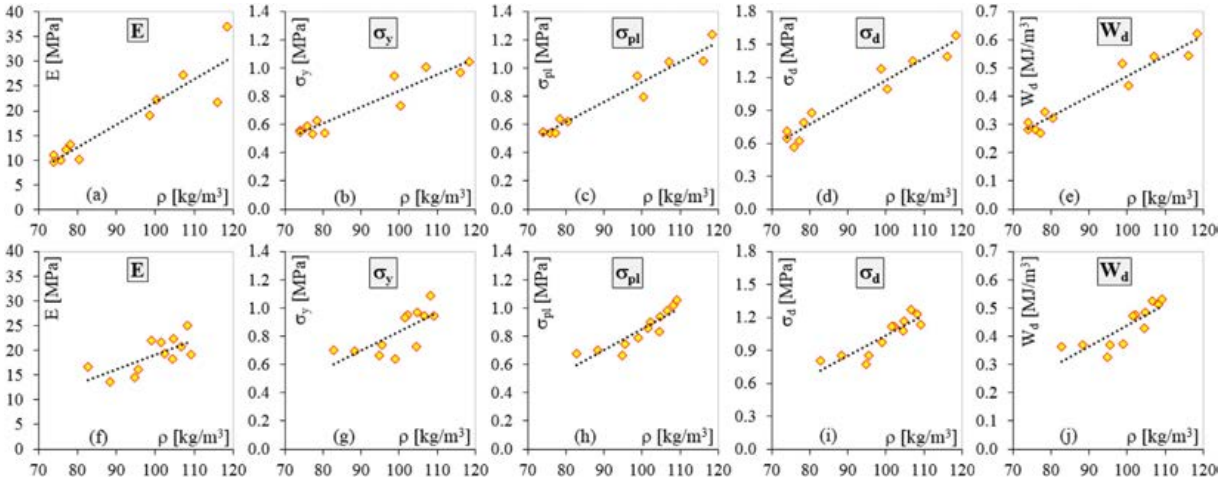

Fig. 14. Variation of main properties (E, σ_y, σ_{pl}, σ_d and W_d,) with density (ρ) for UR/PU (a-e) and GR/PU (f-j) foams.

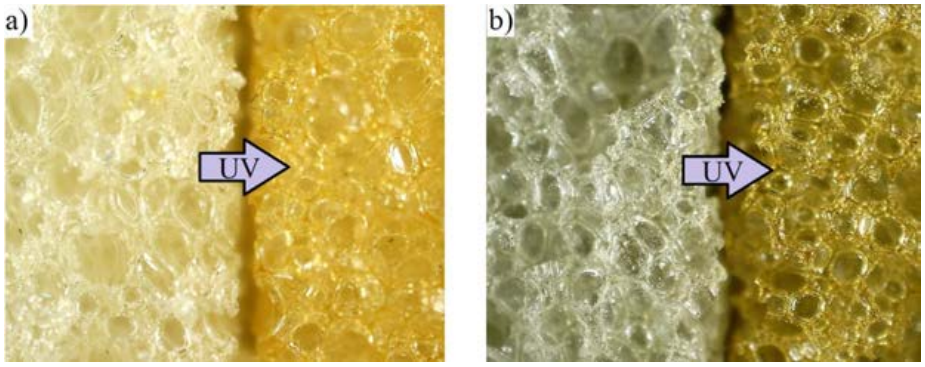

Fig. 15. Comparison of the color change of the UR/PU (a) and GR/PU (b) specimens before and after exposure to UV for 96 h irradiation.

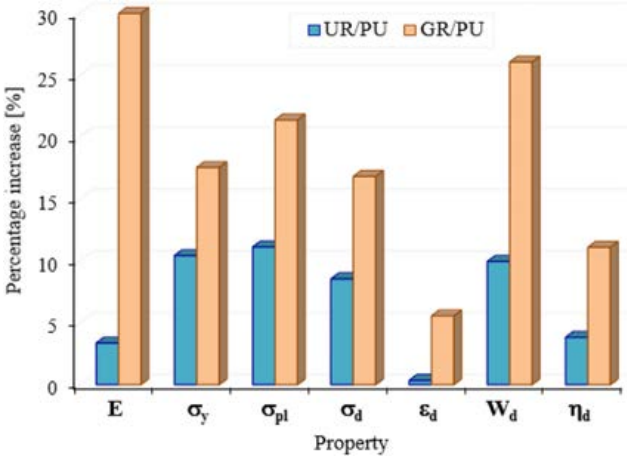

Fig. 16. Percentage increase of foams properties after UV tests.

absorption (energy absorption at densification) performances of investigated foams with sample density.

It can be seen that the UR/PU foams highlight much better grouping of results in comparison to the GR/PU ones that have a relatively high dispersion. This large dispersion of the results can be attributed to the irregular distribution of graphene in the mass of the samples as the density of the foam increases. It can be easily observed that all the investigated properties increase significantly with increasing foam density. Therefore, it can be concluded that the density plays a significant role in determining the compression behavior of the UR/PU and GR/PU foams [59,60]. In the case of most properties, this increase can be associated as being linear with foam density.

The ultraviolet (UV) exposure can cause significant changes to the main properties and useful life of an engineering material. The stability of the composite during UV irradiation is important. The structure can be exposed to UV especially during the manufacturing due to curing some additional layers, and sometimes during operation and maintenance. In the literature, some instabilities of color of polyurethane coatings and PU foams are widely reported. In [61] the foam samples are subjected as a sensor/indicator of UV radiation dose received. Following the exposure of a foam to a UV irradiation of 300–380 nm, Stragliotto and co-workers [61] observed a strong reduction of compressive modulus and increasing of critical strain. Furthermore, Oliviero et al [62] used different percentages of vegetable tannin (0 to 40 wt%) to promote the stabilization of polyurethane foams against UV radiation. They observed that a certain amount of tannin (higher than 20%) leads to improvement of mechanical properties of foams subjected to UV radiation.

In order to highlight the influence of UV radiation on the compression behavior of the UR/PU and GR/PU foams, UV tests were performed. A comparison of the color change of the specimens before and after exposure to UV irradiation is presented in Fig. 15.

Fig. 16 shows the percentage change of the properties of the two foams after UV tests. It is interesting that both foams showed the increase of the properties following the UV tests rather than the deterioration of them, as we would have expected. Moreover, the densities of the foams exposed to UV radiation tests showed values below 1% lower than the initial ones (0.46% for UR/PU and 0.73% GR/PU foams).

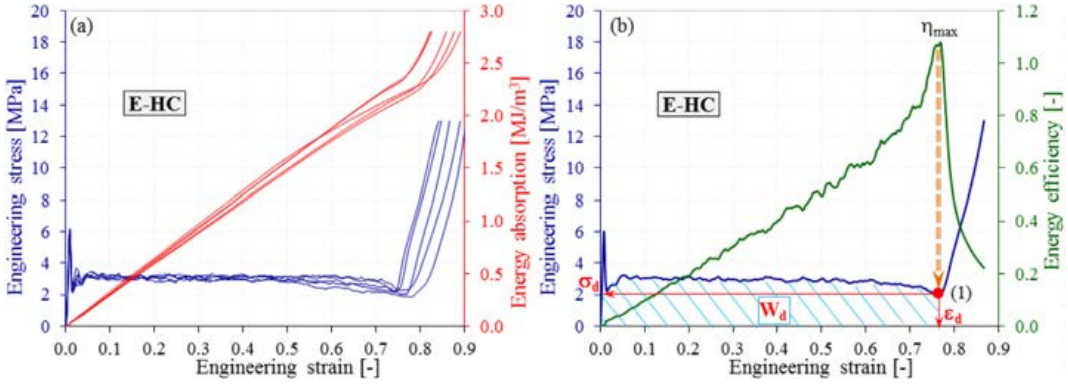

Fig. 17. Stress/energy absorption-strain (a) and stress/energy efficiency-strain (b) curves of E-HC structures.

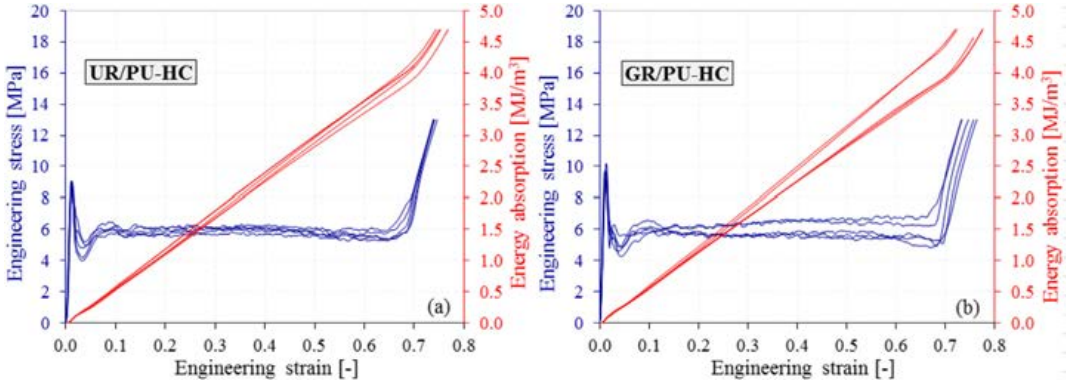

Fig. 18. Stress-strain and energy absorption-strain curves of UR/PU-HC (a) and GR/PU-HC (b) composites.

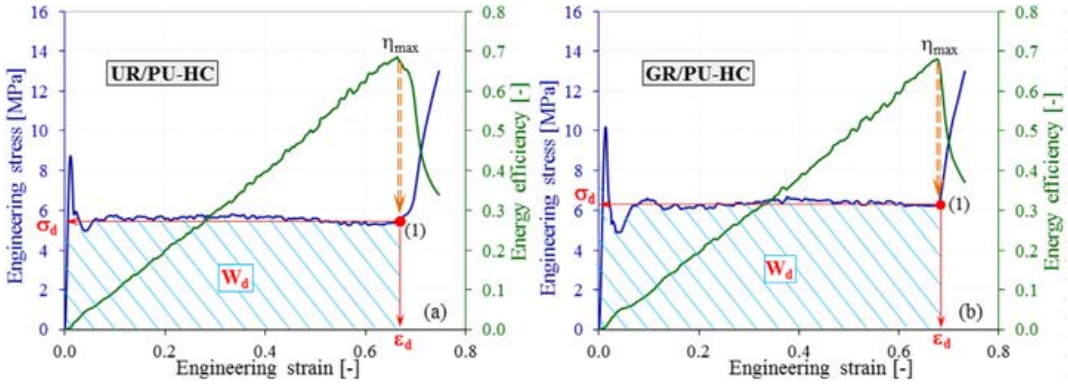

Fig. 19. Stress-strain and energy efficiency-strain curves of UR/PU-HC (a) and GR/PU-HC (b) composites.

Table 5
Main quasi-static properties of E-HC structure.

Foam type	Sample number	E [MPa]	σ_y [MPa]	σ_{pl} [MPa]	σ_d [MPa]	ε_d [%]	W_d [MJ/m^3]	η_d [–]
E-HC	E-HC1	930.414	6.082	3.254	2.179	73.45	2.346	1.077
	E-HC2	893.635	6.179	3.227	1.864	77.97	2.251	1.208
	E-HC3	930.013	5.979	2.887	2.204	73.94	2.107	0.956
	E-HC4	928.353	6.083	3.201	2.364	75.14	2.326	0.984
	E-HC5	938.629	6.029	3.071	2.049	76.83	2.211	1.079

According to Fig. 16, the highest percentage increase, for all properties, was obtained in the case of GR/PU foams. The compressive modulus showed the highest increase of about 30%, while UR/PU foams presented only 3.36%. The strength properties (σ_y, σ_{pl} and σ_d) show smaller increases compared to the elastic ones (E) for GR/PU foams (between 17 and 20%), whereas respectively higher for UR/PU foams (between 9 and 11%). In terms of energy absorption at densification strain (W_d), it has values up to 26.09% higher for GR/PU foams, compared to UR/PU foams, which have only 9.97%. As a general conclusion, when comparing the two foams, it was found that the percentage difference is up to 88.79% higher in favor of reinforced foams.

3.2.2. Honeycomb structures

The response to applied compressive loadings for HC structures is shown in Figs. 17a and 18. From these figures, it can be seen that the HC samples highlight the same three regions (linear elastic, plateau and densification regions) as the ones mentioned in the case of PU foams. By analyzing the σ-ε curves, it can be observed that the linear elastic region ends with an obvious peak point which is located much higher than the plateau region. After the peak stress, a stress drop is found, called stress amplitude (Δσ). Due to progressive deformation and low strength, this Δσ feature could not be established in the case of PU foams. Also, the beginning of the densification strain of E-HC structure takes place after the continuous decrease of the stress on the plateau region (see Fig. 17a). In this case, the hardening of this region is replaced by a progressive softening. This softening of the σ-ε curve is guided by the perpetual buckling of the HC cells. As it can be observed in Fig. 18, this buckling is significantly reduced in the presence of the PU foam inside the HC cells. It seems that due to the interaction effect between the foam and the HC cell walls, the collapse mechanisms is more stable. In addition, due to the high-strength properties of the solid material (aluminum alloy), the densification region of all empty and filled HC structures is much steeper (abrupt) compared to PU foams.

Figs. 17b and 19 show the σ-ε and W-ε curves, respectively the way of determining the densification strain for E-HC, UR/PU-HC and GR/PU-HC structures. The process is the same as the one presented in the case of PU foams, here only the size of the investigated parameters differs.

The main properties of the empty and foam-filled HC structures are collected in Tables 5 and 6, being explained and compared in detail in the following.

The comparison of stress-strain and energy absorption-strain curves is shown in Fig. 20, using the most representative curve in the same sample group (E-HC, UR/PU-HC and GR/PU-HC). Significant

Table 6
Main quasi-static properties of UR/PU-HC and GR/PU-HC composites.

Foam type	Sample number	E [MPa]	σ_y [MPa]	σ_{pl} [MPa]	σ_d [MPa]	ε_d [%]	W_d [MJ/m^3]	η_d [–]
UR/PU-HC	UR/PU-HC1	1115.258	8.834	5.966	5.371	65.00	3.823	0.712
	UR/PU-HC 2	1107.418	8.726	5.634	5.395	66.36	3.698	0.685
	UR/PU-HC 3	1138.097	9.036	6.026	5.281	64.70	3.804	0.720
	UR/PU-HC 4	1103.968	8.874	6.090	5.914	64.54	3.830	0.648
	UR/PU-HC 5	1191.953	9.087	5.934	5.763	64.57	3.724	0.646
GR/PU-HC	GR/PU-HC 1	1290.397	9.751	5.877	4.837	67.12	3.783	0.782
	GR/PU-HC 2	1111.368	9.131	5.681	4.933	68.14	3.835	0.777
	GR/PU-HC 3	1167.455	10.194	6.432	6.271	67.62	4.267	0.680
	GR/PU-HC 4	1107.348	9.677	6.351	6.775	66.09	4.189	0.618
	GR/PU-HC 5	1123.329	9.173	5.667	5.080	69.35	3.858	0.759

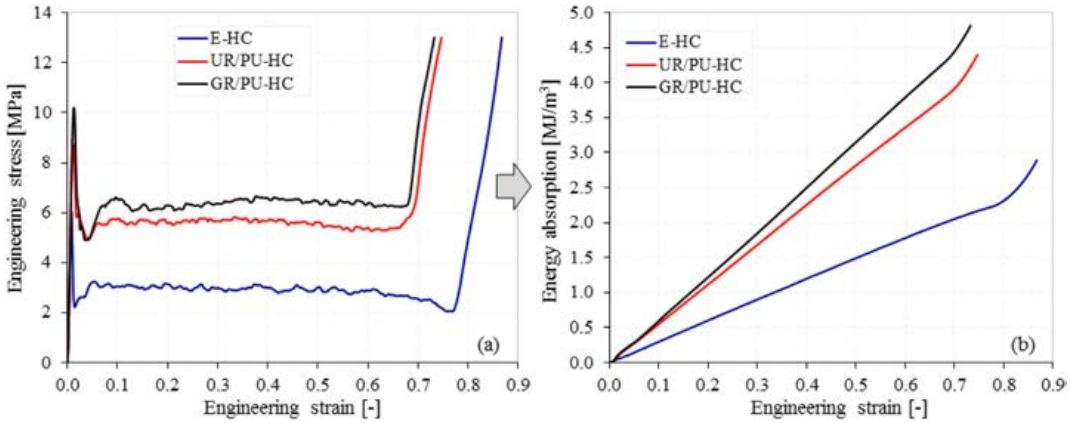

Fig. 20. Stress-strain (a) and energy absorption-strain (b) curves of E/HC, UR/PU-HC and GR/PU-HC structures.

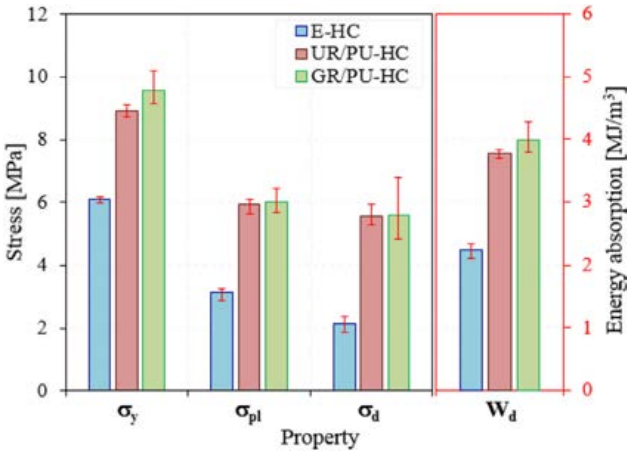

Fig. 21. Strength and energy absorption properties of E/HC, UR/PU-HC and GR/PU-HC structures.

differences were obtained between all three types of HC structures, especially between the empty HC and the filled ones.

Fig. 21 presents a comparison of the strength and energy absorption properties of empty and foam-filled HC structures. The largest differences, over 61% and 47%, were obtained in the case of σ_d and σ_{pl}. These differences have decreased to around 41% (for W_d) and 20% (for E), respectively.

Comparing the two different filled HC composites, it was found that the type of foam does not significantly influence the main mechanical properties. As shown in Fig. 21, the plateau and densification stresses are almost equal, while GR/PU-HC absorbs up to 5.28% more energy than UR/PU-HC structures. On the other hand, the highest increase is obtained in terms of maximum compressive strength, where GR/PU-HC has values higher than UR/PU-HC by about 7%. Therefore, in the case of UR/PU-HC and GR/PU-HC composite structures, due to the higher strength of the HC material, the compression behavior is mostly governed by the HC structure and less by the PU foam.

The quasi-static compression test indicates that in comparison to E-HC much higher energy is needed in order to achieve full collapse of foamed HC. Fig. 22 shows the empty and filled HC specimens after impact tests with the same falling mass. The foamed HC specimen is more resistant than corresponding empty HC.

The deflections are not measured, but they are computed by using following Eq. (4).

$$U(t) = \int v(t)dt = \frac{1}{2}gt^2 - \frac{1}{m}\iint p(t)dtdt \tag{4}$$

where $p(t)$ is measured load, m is a total dropped mass, g is the gravitational acceleration and t is time. The strains of the specimens are computed by assuming the base as the specimen height.

Fig. 23 presents the obtained stress-strain and energy absorption-strain curves of empty and foam-filled HC structures after impact tests. The impact behavior highlights the same three regions characteristic to cellular materials: linear-elastic, plateau and densification regions [44–46].

From Fig. 23 it can be easily seen that the behavior of empty HC structure is much smaller than the corresponding UR/PU-HC and GR/PU-HC, while between foam-filled HC composites there is a very small difference in both σ-ε and W-ε terms. Due to the inertia effect, the plateau region presents oscillations of different shapes and sizes. These oscillations are less pronounced for empty HC and more obvious

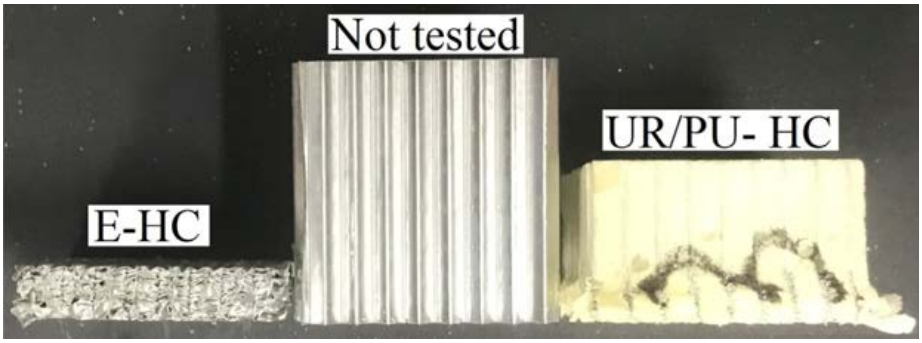

Fig. 22. Initial / damaged empty and foam-filled HC specimens.

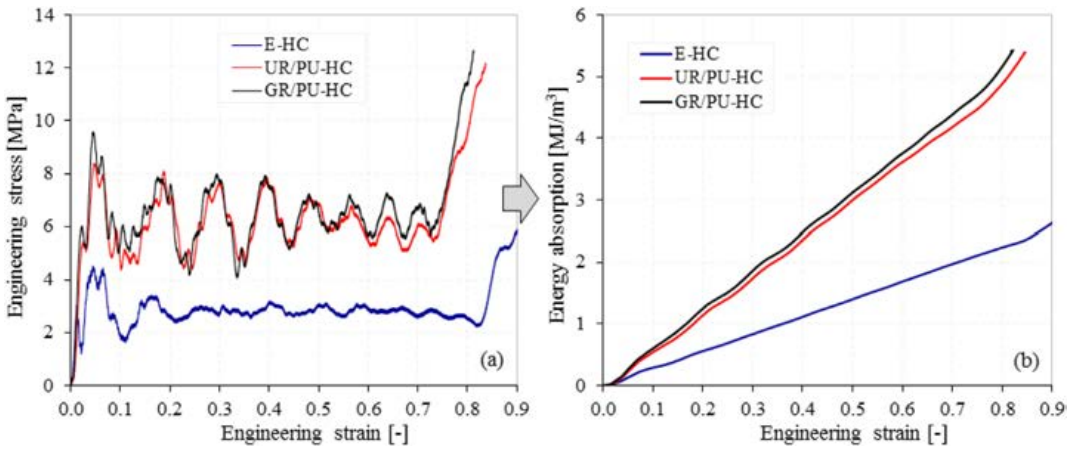

Fig. 23. Stress-strain (a) and energy absorption-strain (a) curves of E-HC, UR/PU-HC and GR/PU-HC structures after impact tests.

Table 7
Main impact properties of E-HC, UR/PU-HC and GR/PU-HC structures.

Foam type	Sample number	σ_y [MPa]	σ_d [MPa]	ε_d [%]	W_d [MJ/m^3]	η_d [–]
E-HC	E-HC 1	5.015	1.741	83.27	2.313	0.991
	E-HC 2	5.067	2.334	80.39	2.303	1.110
	E-HC 3	4.550	2.075	82.02	2.289	1.029
	E-HC 4	5.032	2.224	81.36	2.292	0.975
	E-HC 5	4.535	2.352	82.56	2.377	1.415
UR/PU-HC	UR/PU-HC 1	9.054	5.832	72.44	4.566	0.783
	UR/PU-HC 2	8.895	5.561	73.59	4.532	0.815
	UR/PU-HC 3	8.402	5.427	73.14	4.367	0.805
	UR/PU-HC 4	8.398	5.559	72.20	4.440	0.799
	UR/PU-HC 5	8.404	6.099	71.97	4.494	0.737
GR/PU-HC	GR/PU-HC 1	9.711	5.531	74.38	4.368	0.790
	GR/PU-HC 2	8.963	5.466	74.83	4.407	0.795
	GR/PU-HC 3	8.380	5.547	72.34	4.815	0.693
	GR/PU-HC 4	10.066	5.674	72.61	4.555	0.803
	GR/PU-HC 5	9.593	5.775	73.04	4.587	0.794

for filled HCs. On the other hand, empty HC has a much larger plateau region compared to filled structures. The main properties of the 3 types of HC structures (E-HC, UR/PU-HC and GR/PU-HC), following the impact tests, are listed in Table 7.

The foam-filled HC structures presents compressive strength values up to 48% higher than non-filled ones. Even if the E-HC densification strain (ε_d) starts much later (almost 82% for E-HC compared to 73% for filled HC), foam-filled composites have almost double energy absorption values.

Fig. 24 presents a comparison of quasi-static and impact stress-strain curves of investigated E/HC, UR/PU-HC and UR/PU-HC structures. In the same figure, there is a comparison of the compressive strength and the absorption energy for the two types of tests.

The σ-ε curves exhibit a very different shape depending on the type of test (Fig. 24a-c). The specimens tested under quasi-static loading conditions have a higher stiffness than those tested at impact. In addition, the quasi-static tests highlights a much more stable defamation mechanisms of the specimens compared to the impact ones (lack of oscillations on the plateau area), while the length of this region is higher in the case of impact tests. For all types of HC structures, the compressive strength is higher for quasi-static tests. The biggest difference, of 20.27%, is obtained in the case of empty HC structures, foam-filled composites presenting a difference of only 3%. On the contrary, due to the size of the plateau region and the delayed beginning of the densification strain, the impact tests have higher values of the energy absorption (Fig. 24d-f). In this case, the filled HC structures absorb more energy (up to 18.5%) compared to empty ones, which absorbs only 2.95% more in the case of impact tests.

3.3. Collapse mechanisms

The compression strength in such structures is determined by the material, ribbons thickness and cell shape, as well as the initial imperfection of geometry. To check the distribution of strains, just before the start the progressive collapsing of HC in compressive tests, a digital image correlation (DIC) system was used. The normal strain ε_{yy} in load direction distribution at peak point of loading force is presented in Fig. 25.

The structure is uniformly strained before reach the critical value of loading force. Just before the collapsing, the strain distribution indicates the chessboard like regular pattern of positive and negative values. This pattern shows that the ribbon is deformed to wave shape, in similar way like the imperfection due to manufacturing process, which are visible in unloaded product. The initial height of the considered HC panel is 40 mm; we can observe the 7 waves which means that this wave length is approximately 5.7 mm. The waves distributions correspond to distributions of dent shape imperfections, which are visible in Fig. 2.

The huge differences in collapse mode of empty HC and filled by PU foams are observed. This phenomenon is responsible for high-energy absorption increase of HC after the filling by PU foam.

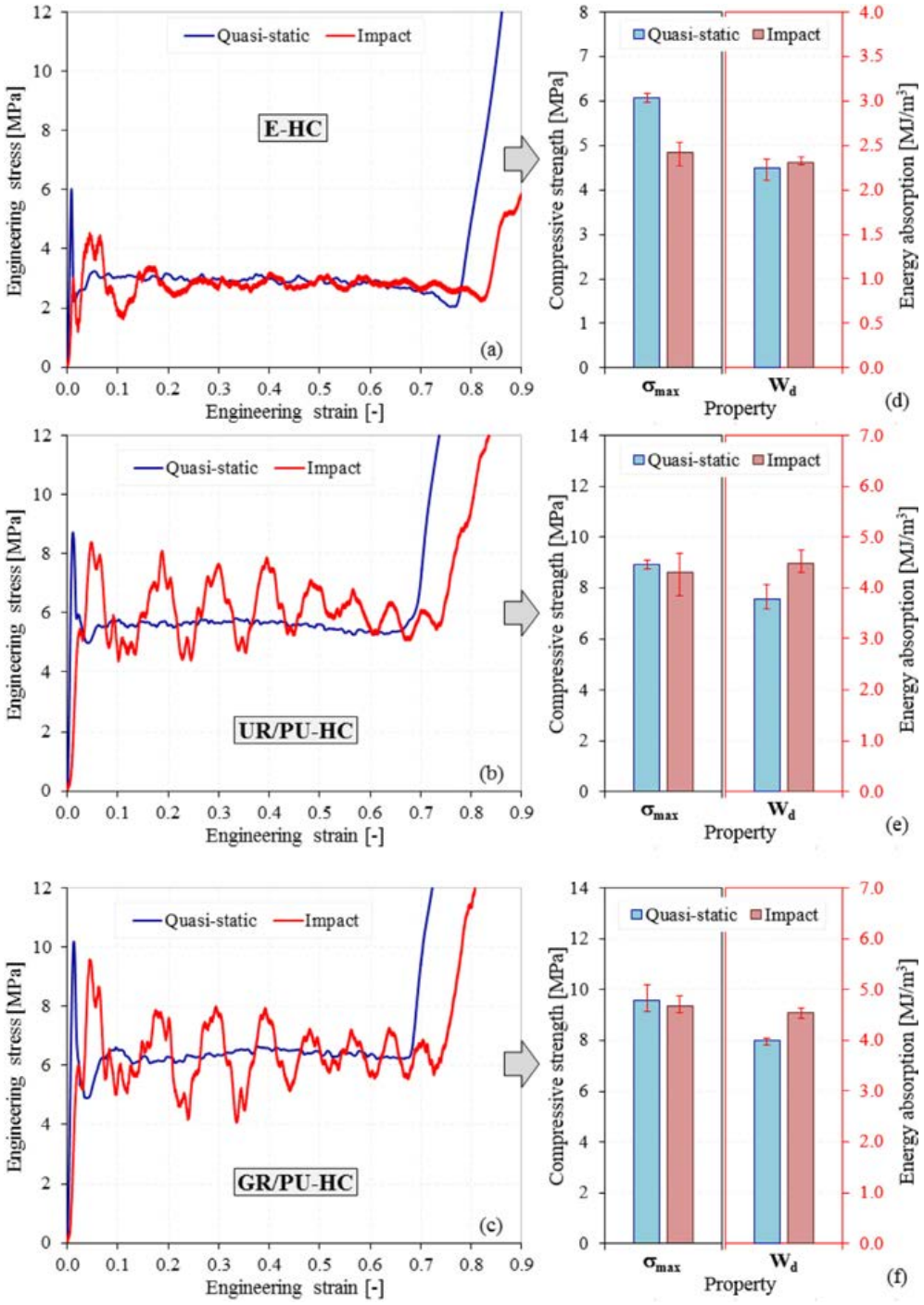

Fig. 24. Stress-strain (a-c) curves and properties variation (d-f) of E/HC, UR/PU-HC and UR/PU-HC structures under quasi-static and impact tests.

Both empty and foamed HC indicates the progressive collapsing during the compression tests. The history of collapsing is stored in their cross section. Therefore, in this study, to investigate the cells walls buckling process the compressed specimens were cut into smaller part to obtain desired cross sections. The specimens were included into the polyester resin so as to protect the delicate foam and aluminum structure against damage by the cutting wheel. The specimen was cut in ribbon direction and perpendicular to ribbon direction to achieve cross-sections in the most characteristic points of HC structure especially in double wall section, and through the cells. Fig. 26 presents 4 possible sections, which can be obtained after compression tests.

In the case of empty HC after the compressive test, the height was reduced to approximately 4.8 mm as shown in the Figs. 27–29. In the same test conditions, the foamed specimen was been pressed to height 10.6 mm (see Fig. 25). In Fig. 27, collapsing of the single ribbon cell walls is visible. In this case, the walls collapse separately and between them are no contact occurs; there exists only the self-contact of buckled parts of the cell walls. The self-contact occur only in E-HC specimen. In the foam-filled HC, the arrangement of folds is regular. In E-

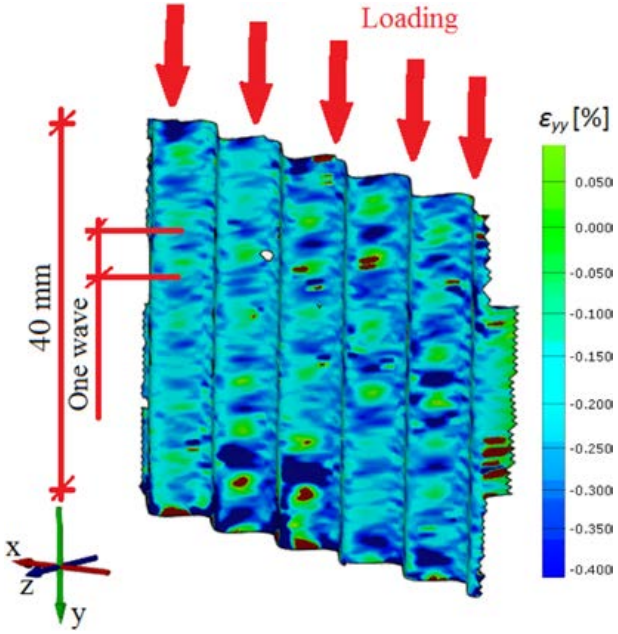

Fig. 25. The normal strain in loading direction at peak value of force.

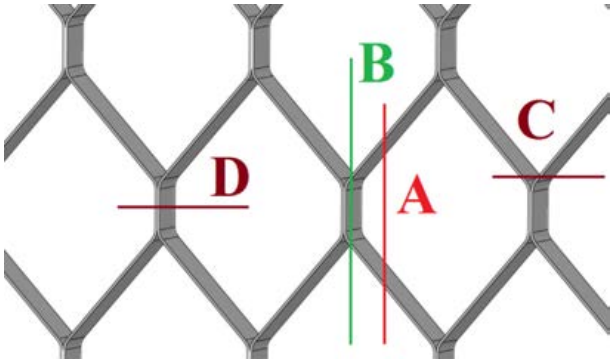

Fig. 26. The positions of considered cross-sections.

HC it can be found approximately the same number of folds (~16) in both kinds of specimens, which corresponds to the number of waves which are visible in Fig. 25.

As shown in Fig. 28 in the part that is close to the ribbons joint, in cross-section "B", the buckled walls touch each other in both kinds of specimen. Similarly, like in case of cross section A the foamed HC specimen, the folds are more regular than in empty HC specimen. In this case, the folds are interwoven with each other.

In the case of cross-section "C", performed in the vicinity of the bonding of the HC ribbons, the folds are situated in reverse, due to this fact they are do not intertwined, as shown in Fig. 29. This phenomenon is clearly visible in the foamed HC specimen. In empty HC specimen, narrowing is visible in the middle of their height.

In section "D", Fig. 30, we can observe the collapsing of double ribbons of HC structure. From the numerical modeling point of view, it is necessary to observe the behavior of the ribbon-ribbon joint as to find some delaminated areas. In the case of empty HC, it is important to check the buckling of double walls. The unbounded regions are visible only in empty HC structure at the tips of the folds. The empty HC specimen is fully compressed. Moreover, in the upper part the shearing of the compressed ribbons is visible. In the foam-filled HC specimens, the distances between uncompressed folds are approximately equal.

In addition, in collapsed HC structure are also visible broken ribbons as shown in Fig. 31. These broken ribbons lead to the weakening of the structure resistance and directly influence the shape of the stress-strain curve and implicitly of the properties.

4. Conclusions

In this paper, the modern aluminum honeycomb (HC) panels filled with unreinforced (UR) and graphene-reinforced (GR) polyurethane (PU) foams were investigated. The response of these foam-filled HC composite structures were tested under quasi-static and low velocity impact out-of-plane compressive tests. The stability of the UR/PU and GR/PU foams exposed to ultraviolet (UV) irradiation was also considered. Two manufacturing methods and the collapse mechanisms of the foam-filled HC panels are presented. The obtained results are compared to the response of separate composite constituents and their various combination (i.e. UR foam, GR foam, empty HC and foam-filled HC).

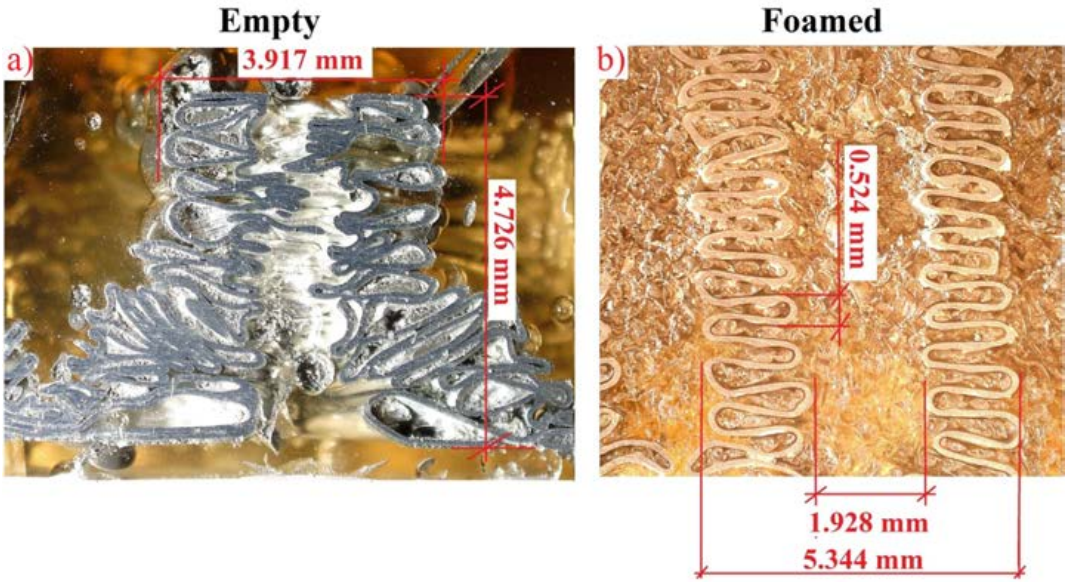

Fig. 27. The cross section "A" in collapsed empty HC structure (a) and foam-filled HC (b).

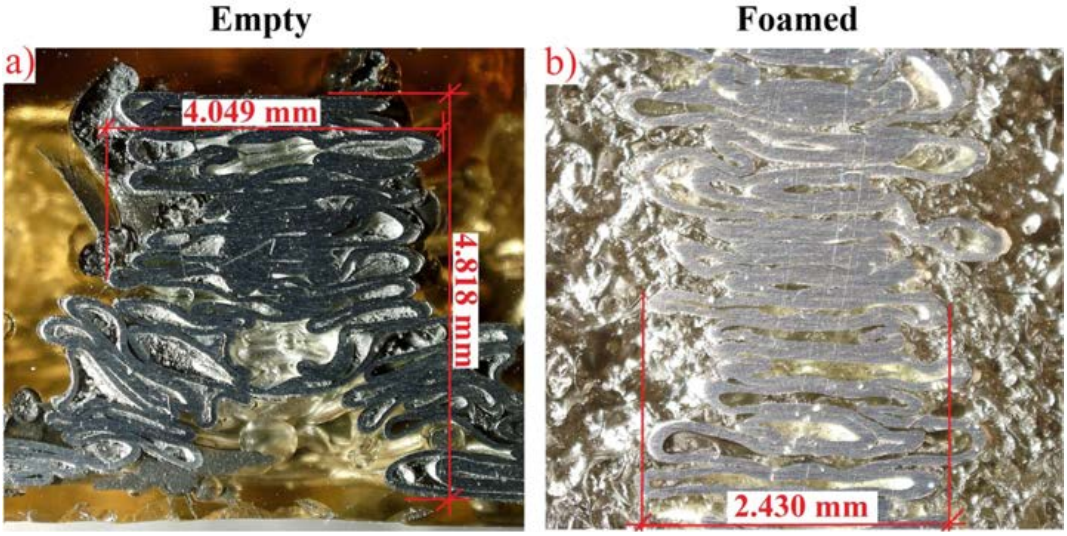

Fig. 28. The cross Section "B" in collapsed empty HC structure (a) and foam-filled HC (b).

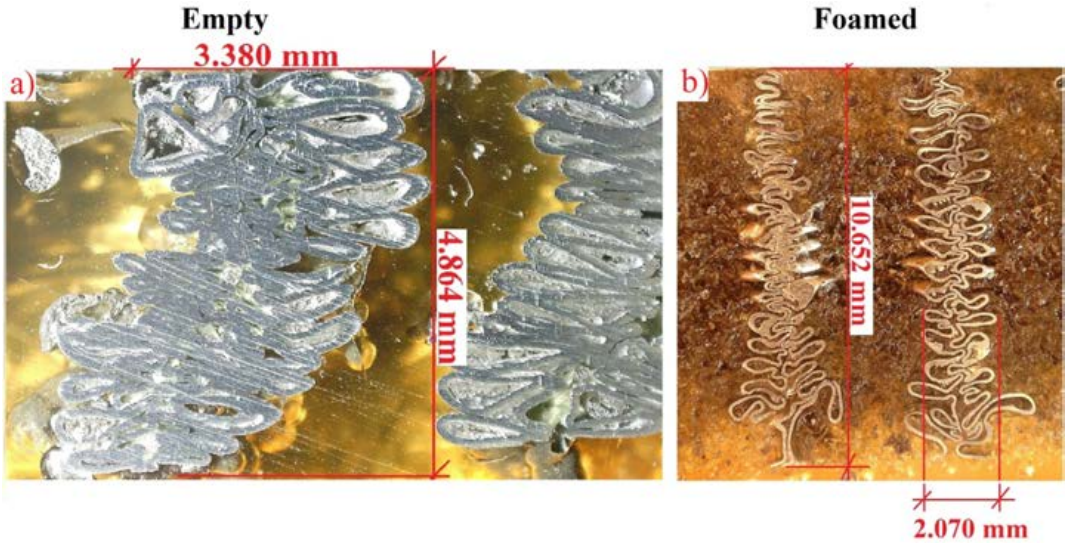

Fig. 29. The cross Section "C" in collapsed empty HC structure (a) and foam-filled HC (b).

It has been observed that the *in-situ* method (growth of the PU foam inside the HC cells) is much more favorable than the corresponding *ex-situ* method (mechanically pressing of the PU foam through the HC cells). The *ex-situ* method leads to the appearance of different micro and macro defects (voids between the PU foam-HC walls interface, foam indentation regions, changes in foam cell shape, etc.), while for the *in-situ* method these shortcomings are eliminated due to the strong bonding effect between foam and HC walls.

The achieved results indicate that the addition of 0.02% reduced graphene oxide (rGO) flakes in the mass of the liquid foam constituents leads to an increase of strength properties and energy absorption capacity of over 41%. Moreover, due to the interaction between the foam and the HC cell-walls, the main mechanical properties of the foam-filled HC composite are up to 61% higher than that of the empty HC structure. In addition, it was discovered that the UV exposure, for a period of 96 h, leads to an increase of the main properties (up to 30%), without a significant change in foam density (below 0.8%). Finally, it was observed that the foam, as a filling material, considerably governs the HC collapse mechanisms.

A corresponding numerical model of crushing process of the considered HC filled with PU and GR will be formulated using FEM approach [14–21] with different degradation processes described in [63–71].

CRediT authorship contribution statement

Daniel Pietras: Conceptualization, Writing - original draft, Writing - review & editing, Visualization, Formal analysis, Methodology. **Emanoil Linul:** Conceptualization, Writing - original draft, Writing - review & editing, Visualization, Formal analysis, Methodology. **Tomasz Sadowski:** Conceptualization, Investigation, Writing - original draft, Writing - review & editing, Visualization, Formal analysis, Methodology. **Alexis Rusinek:** Conceptualization, Investigation, Writing - review & editing, Formal analysis, Methodology.

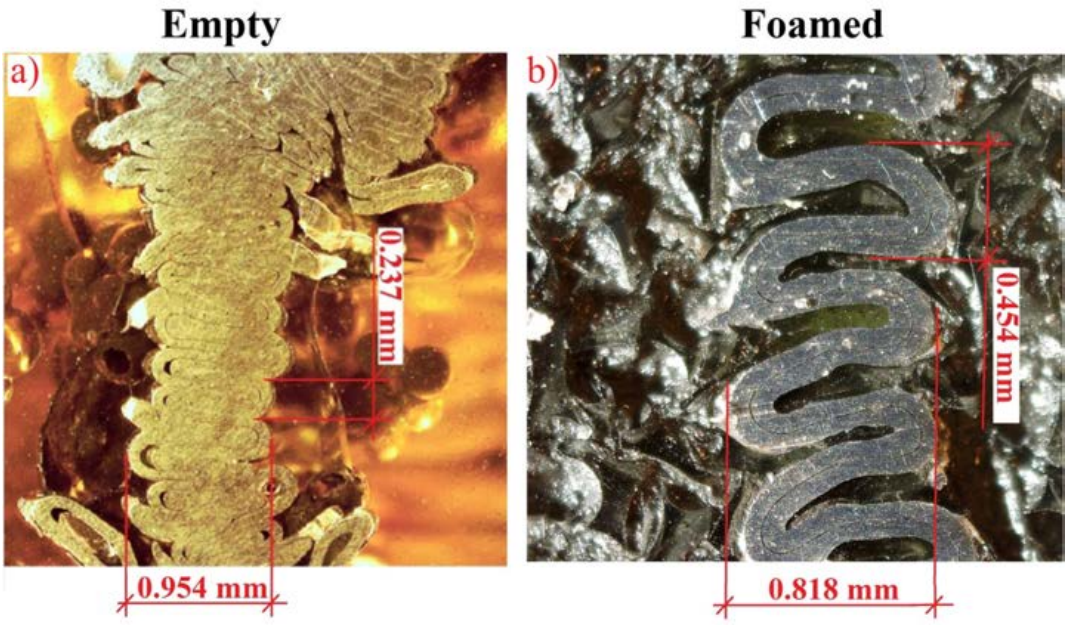

Fig. 30. The cross Section "D" in collapsed empty HC structure (a) and foam-filled HC (b).

Fig. 31. The broken ribbon during the compression test.

Declaration of Competing Interest

The authors declare that they have no known competing financial interests or personal relationships that could have appeared to influence the work reported in this paper.

Acknowledgement

This research was funded by National Science Centre, Poland, grant "Miniatura 2" 2018/02/X/ST8/01842.

The reduced graphene oxide (rGO) flakes, manufactured by Institute of Electronic Materials Technology (Warsaw, Poland) were provided by Dr. M. Boniecki.

Appendix A. Supplementary data

Supplementary data to this article can be found online at https://doi.org/10.1016/j.compstruct.2020.112548.

References

[1] Wang Z. Recent advances in novel metallic honeycomb structure. Compos B Eng 2019;166:731–41.
[2] Wang Z, Liu J. Numerical and theoretical analysis of honeycomb structure filled with circular aluminum tubes subjected to axial compression. Compos B Eng 2019;165:626–35.
[3] Birsan M, Sadowski T, Marsavina L, et al. Mechanical behavior of sandwich composite beams made of foams and functionally graded materials. Int J Solid Struct 2013;50:519–30.
[4] Voiconi T, Linul E, Marsavina L, et al. Determination of flexural properties of rigid PUR foams using digital image correlation. Solid State Phenom 2014;216:116–21.
[5] Burlayenko V, Sadowski T. A numerical study of the dynamic response of sandwich plates initially damaged by low-velocity impact. Comput Mat Sci 2012;52:212–6.
[6] Zhang C, Li A, Zhao YH, et al. Thermal, electrical and mechanical properties of graphene foam filled poly(methyl methacrylate) composite prepared by in situ polymerization. Compos B Eng 2018;135:201–6.
[7] Li J, Zhang A, Zhang S, et al. Larch tannin-based rigid phenolic foam with high compressive strength, low friability, and low thermal conductivity reinforced by cork powder. Compos B Eng 2019;156:368–77.
[8] Linul E, Vălean C, Linul PA. Compressive behavior of aluminum microfibers reinforced semi-rigid polyurethane foams. Polymers 2018;10(12):1298.
[9] Movahedi N, Murch GE, Belova IV, Fiedler T. Manufacturing and compressive properties of tube-filled metal syntactic foams. J Alloy Compd 2020;822:153465.
[10] Linul E, Movahedi N, Marsavina L. The temperature effect on the axial quasi-static compressive behavior of ex-situ aluminum foam-filled tubes. Compos Struct 2017;180:709–22.
[11] Movahedi N, Linul E. Quasi-static compressive behavior of the ex-situ aluminum-alloy foam-filled tubes under elevated temperature conditions. Mater Lett 2017;206:182–4.
[12] Santosa SP, Wierzbicki T, Hanssen AG, Langseth M. Experimental and numerical studies of foam-filled sections. Int J Impact Eng 2000;24:509–34.
[13] Kavi HA, Toksoy K, Guden M. Predicting energy absorption in a foam-filled thin-walled aluminum tube based on experimentally determined strengthening coefficient. Mater Des 2006;27(4):263–9.
[14] Zarei MM, Sadighi M. A study on the static and dynamic loading of the foam filled metal hexagonal honeycomb – theoretical and experimental. Mat Sci Eng A-Struct 2011;530:333–43.
[15] Caliri Mauricio F, Jr A, Ferreira JM. Tita V. A review on plate and shell theories for laminated and sandwich structures highlighting the Finite Element Method. Comp Struct 2016;156:63–77.
[16] Belinha J, Araújo AL, Ferreira AJM, Dinis LMJS, Natal Jorge RM. The analysis of laminated plates using distinct advanced discretization meshless techniques. Comp Struct 2016;143:165–79.
[17] Burlayenko VN, Altenbach H, Sadowski T. An evaluation of displacement-based finite element models used for free vibration analysis of homogeneous and composite plates. J Sound Vib 2015;358:152–75.
[18] Burlayenko VN, Pietras D, Sadowski T. Influence of geometry, elasticity properties and boundary conditions on the Mode I purity in sandwich composites. Comp Struct 2019;223:110942.

[19] Craciun EM, Carabineanu A, Peride N. Antiplane interface crack in a pre-stressed fiber-reinforced elastic composite. Comp Mater Sci 2012;43(1):184–9.
[20] Sadowski T, Marsavina L, Peride N, Craciun EM. Cracks propagation and interaction in an orthotropic elastic material: analytical and numerical methods. Comput Mat Sci 2009;46:687–93.
[21] Marsavina L, Nurse AD, Braescu L, Craciun EM. Stress singularity of symmetric free-edge joints with elasto-plastic behavior. Comp Mater Sci 2012;52:282–6.
[22] Deqiang S, Weihong Z, Yanbin W. Mean out-of-plane dynamic plateau stresses of hexagonal honeycombcores under impact loadings. Compos Struct 2010;92:2609–21.
[23] Tao Y, Chen M, Pei Y, Fang D. Strain rate effect on mechanical behavior of metallic honeycombs under out-of-plane dynamic compression. J Appl Mech 2015;82 (2):021007.
[24] Xu S, Beynon JH, Ruan D, Lu G. Experimental study of the out-of-plane dynamic compression of hexagonal honeycombs. Compos Struct 2012;94:2326–36.
[25] Guo WG, Zhang XQ, Sua J, Sub Y, Zeng ZY, Shao XJ. The characteristics of plastic flow and a physically-based model for 3003 Al-Mn alloy upon a wide range of strain rates and temperatures. Eur J Mech A-Solid 2011;30:54–62.
[26] Stanczak M, Fras T, Blanc L, Pawlowski P, Rusinek A Numerical modelling of honeycomb structure subjected to blast loading 12thEuropean LS-DYNA Conference 2019, Koblenz, Germany.
[27] Zhong W, Rusinek A, Jankowiak T, Huang X, Abed F. Experimental and numerical investigation on compression orthotropic properties of spruce wood in axial and transverse loading directions. Eng Trans 2014;62(4):381–401.
[28] Strankowski M, Korzeniewski P, Strankowska J, Anu AS, Thomas S. Morphology, mechanical and thermal properties of thermoplastic polyurethane containing reduced graphene oxide and graphene nanoplatelets. Materials 2018;11:1–18.
[29] Santiago-Calvo M, Blascob V, Ruiz C, París R, Villafañe F, Rodríguez-Pérez MÁ. Synthesis, characterization and physical properties of rigid polyurethane foams prepared with poly(propylene oxide) polyols containing grapheneoxide. Eur Polym J 2017;97:230–40.
[30] Yan D, Xu L, Chen C, Tang J, Ji X, Li Z. Enhanced mechanical and thermal properties of rigid polyurethane foam composites containing graphene nanosheets and carbon nanotubes. Polym Int 2012;61:1107–14.
[31] Liu HD, Liu ZY, Yang MB, He Q. Surperhydrophobic polyurethane foam modified by graphene oxide. J Appl Polym Sci 2013;130:3530–6.
[32] Hodlur RM, Rabinal MK. Self assembled graphene layers on polyurethane foam as a highly pressure sensitive conducting composite. Compos Sci Technol 2014;90:160–5.
[33] Piszczyk Ł, Kosmela P, Strankowski M. Elastic polyurethane foams containing graphene nanoplatelets. Adv Polymer Technol 2017;00:1–10. https://doi.org/10.1002/adv.21819.
[34] Sadowski T, Bęc J. Effective properties of sandwich plates with aluminum foil honeycomb and polymer foam filling - Static and dynamic response. Comp Mater Sci 2011;50:1269–75.
[35] Linul E, Movahedi N, Marsavina L. On the lateral compressive behavior of empty and ex-situ aluminum foam-filled tubes at high temperature. Materials 2018;11 (4):554.
[36] Rajak DK, Mahajan NN, Linul E. Crashworthiness performance and microstructural characteristics of foam-filled thin-walled tubes under diverse strain rate. J Alloy Compd 2019;775:675–89.
[37] Pietras D, Sadowski T. Parametric study of geometry effect on response to applied loadings of metallic honeycomb structures by virtual testing of mesoscale models. Arch Metall Mater 2018;63(2):953–61.
[38] Liu S, Tian J, Wang L, Sun X. A method for the production of reduced graphene oxide using benzylamine as a reducing and stabilizing agent and its subsequent decoration with Ag nanoparticles for enzymeless hydrogen peroxide detection. Carbon 2011;49:3158–64.
[39] Kumar P, Subrahmanyam KS, Rao CNR Graphene produced by radiation-induced reduction of graphene oxide. Int. J. Nanosci. 2011;10:559-566 Special Issue on Nanoscience and Technology (ICONSAT 2010).
[40] Marsavina L, Constantinescu DM, Linul E, et al. Evaluation of mixed mode fracture for PUR foams. Procedia Mater Sci 2014;3:1342–52.
[41] Lee J, Kim J, Shin Y, Jung I. Ultra-robust wide-range pressure sensor with fast response based on polyurethane foam doubly coated with conformal silicone rubber and CNT/TPU nanocomposites islands. Compos B Eng 2019;177:107364.
[42] ISO13314, Mechanical testing of metals — Ductility testing — Compression test for porous and cellular metals, 2011.
[43] ASTM G177 - 03(2012), Standard Tables for Reference Solar Ultraviolet Spectral Distributions: Hemispherical on 37° Tilted Surface.
[44] Fiedler T, Al-Sahlani K, Linul PA, Linul E. Mechanical properties of A356 and ZA27 metallic syntactic foams at cryogenic temperature. J Alloy Compd 2020;813:152181.
[45] Kovácik J, Jerz J, Mináriková N, Marsavina L, Linul E. Scaling of compression strength in disordered solids: metallic foams. Frattura ed Integrita Strutturale 2016;36:55–62.
[46] Sahu S, Mondal DP, Cho JU, Goel MD, Ansari MZ. Low-velocity impact characteristics of closed cell AA2014-SiCp composite foam. Compos B Eng 2019;160:394–401.
[47] Su M, Wang H, Hao H. Axial and radial compressive properties of alumina-aluminum matrix syntactic foam filled thin-walled tubes. Compos Struct 2019;226:111197.
[48] Movahedi N, Linul E, Marsavina L. The temperature effect on the compressive behavior of closed-cell aluminum-alloy foams. J Mater Eng Perform 2018;27 (1):99–108.
[49] Orbulov IN, Kemény A, Filep Á, Gácsi Z. Compressive characteristics of bimodal aluminium matrix syntactic foams. Compos Part A Appl Sci Manuf 2019;124:105479.
[50] Linul E, Marşavina L, Linul PA, Kovacik J. Cryogenic and high temperature compressive properties of Metal Foam Matrix Composites. Compos Struct 2019;209:490–8.
[51] Chen J, Fang H, Liu W, et al. Energy absorption of foam-filled multi-cell composite panels under quasi-static compression. Compos B Eng 2018;153:295–305.
[52] Linul E, Lell D, Movahedi N, Codrean C, Fiedler T. Compressive properties of Zinc Syntactic Foams at elevated temperatures. Compos B Eng 2019;167:122–34.
[53] Zhou J, Guan Z, Cantwell WJ. The energy-absorbing behaviour of composite tube-reinforced foams. Compos B Eng 2018;139:227–37.
[54] Linul E, Şerban DA, Marsavina L, Sadowski T. Assessment of collapse diagrams of rigid polyurethane foams under dynamic loading conditions. Arch Civ Mech Eng 2017;17(3):457–66.
[55] Zhang Y, He SY, Liu JG, et al. Density gradient tailoring of aluminum foam-filled tube. Compos Struct 2019;220:451–9.
[56] Aliha MRM, Mousavi SS, Bahmani A, Linul E, Marsavina L. Crack initiation angles and propagation paths in polyurethane foams under mixed modes I/II and I/III loading. Theor Appl Fract Mec 2019;101:152–61.
[57] Linul E, Marsavina L, Sadowski T, Kneć M. Size effect on fracture toughness of rigid polyurethane foams. Solid State Phenom 2012;188:205–10.
[58] Linul E, Marsavina L, Kovacik J, Sadowski T. Dynamic and quasi-static compression tests of closed-cell aluminium alloy foams. Proceedings of the Romanian Academy – Series A, 2017;18(4):361-369.
[59] Lacki P, Derlatka A, Winowiecka J. Analysis of the composite I-beam reinforced with PU foam with the addition of chopped glass fiber. Compos Struct 2019;218:60–70.
[60] Linul E, Voiconi T, Marsavina L, Sadowski T. Study of factors influencing the mechanical properties of polyurethane foams under dynamic compression. J Phys Conf 2013;451:012002.
[61] Stragliotto MF, Mosconi G, Strumia MC, Romero MR, Gomeza CG. UV sensor based on polyurethane foam. Sens Actuators B Chem 2018;277:78–85.
[62] Oliviero M, Stanzione M, D'Auria M, Sorrentino L, Iannace S, Verdolotti L. Vegetable tannin as a sustainable UV stabilizer for polyurethane foams. Polymers 2019;11(3):480.
[63] Golewski P, Sadowski T. Investigation of the effect of chamfer size on the behavior of hybrid joints made by adhesive bonding and riveting. Int J Adh Adh 2017;77:174–82.
[64] Sadowski T, Golewski P, Kneć M. Experimental investigation and numerical modelling of spot welding-adhesive joints response. Comp Struct 2014;112:66–77.
[65] Sadowski T, Pankowski B. Numerical modelling of two-phase ceramic composite response under uniaxial loading. Comp Struct 2016;143:388–94.
[66] Sadowski T. Gradual degradation in two-phase ceramic composites under compression. Comput Mat Sci 2012;64:209–11.
[67] Ivanov IV, Sadowski T, Pietras D. Crack propagation in functionally graded strip under thermal shock. Eur Phys J Special Topics 2013;222:1587–95.
[68] Sadowski T, Neubrand A. Estimation of the crack length after thermal shock in FGM strip. Int J Fract 2004;127:L135–40.
[69] Burlayenko V, Altenbach H, Sadowski T, Dimitrova SD, Bhaskar A. Modelling functionally graded materials in heat transfer and thermal stress analysis by means of graded finite elements. Appl Math Model 2017;45:422–38.
[70] Marsavina L, Sadowski T. Fracture parameters at bi-material ceramic interfaces under bi-axial state of stress. Computational Materials Science 2009;45(3):603–97.
[71] Sadowski T, Samborski S. Prediction of the mechanical behaviour of porous ceramics using mesomechanical modelling. Computational Materials Science 2003;28(3–4):512–7.